Geochemistry Geophysics Geosystems G3
AN ELECTRONIC JOURNAL OF THE EARTH SCIENCES
Published by AGU and the Geochemical Society

Article
Volume 7, Number 10
7 October 2006
Q10005, doi:10.1029/2006GC001336
ISSN: 1525-2027

Thermochronology of mineral grains in the Red and Mekong Rivers, Vietnam: Provenance and exhumation implications for Southeast Asia

Peter D. Clift
School of Geosciences, University of Aberdeen, Meston Building, Kings College, Aberdeen AB24 3UE, UK (p.clift@abdn.ac.uk)

Andrew Carter
School of Earth Sciences, University and Birkbeck College London, Gower Street, London WC1E 6BT, UK

Ian H. Campbell
Institute of Advanced Studies, Research School of Earth Sciences, Australian National University, Canberra, ACT 0200, Australia

Malcolm S. Pringle
Department of Earth, Atmospheric and Planetary Sciences, Massachusetts Institute of Technology, Cambridge, Massachusetts 02139, USA

Nguyen Van Lap
Sub-Institute of Geography, Vietnamese Academy of Science and Technology, Ho Chi Minh City, Vietnam

Charlotte M. Allen
Institute of Advanced Studies, Research School of Earth Sciences, Australian National University, Canberra, ACT 0200, Australia

Kip V. Hodges
Department of Earth, Atmospheric and Planetary Sciences, Massachusetts Institute of Technology, Cambridge, Massachusetts 02139, USA

Now at School of Earth and Space Exploration, Arizona State University, Tempe, Arizona 85287, USA

Mai Thanh Tan
Hanoi University of Mining and Geology, Dong Ngac, Tu Liem, Hanoi, Vietnam

[1] Sand samples from the mouths of the Red and Mekong Rivers were analyzed to determine the provenance and exhumation history of their source regions. U-Pb dating of detrital zircon grains shows that the main sources comprise crust formed within the Yangtze Craton and during the Triassic Indosinian Orogeny. Indosinian grains in the Mekong are younger (210–240 Ma) than those in the Red River (230–290 Ma), suggesting preferential erosion of the Qiangtang Block of Tibet into the Mekong. The Red River has a higher proportion of 700–800 Ma grains originally derived from the Yangtze Craton. $^{40}Ar/^{39}Ar$ dating of muscovite grains demonstrates that rocks cooled during the Indosinian Orogeny are dominant in both rivers, although the Mekong also shows a grain population cooling at 150–200 Ma that is not seen in the Red River and which is probably of original Qiangtang Block origin. Conversely, the Red River contains a significant mica population (350–500 Ma) eroded from the Yangtze Craton. High-grade

metamorphic rocks exposed in the Cenozoic shear zones of southeast Tibet-Yunnan are minority sources to the rivers. However, apatite and zircon fission track ages show evidence for the dominant sources, especially in the Red River, only being exhumed through the shallowest 5–3 km of the crust since ~25 Ma. The thermochronology data are consistent with erosion of recycled sediment from the inverted Simao and Chuxiong Basins, from gorges that incise the eastern flank of the plateau. Average Neogene exhumation rates are 104–191 m/Myr in the Red River basin, which is within error of the 178 ± 35 m/Myr estimated from Pleistocene sediment volumes. Sparse fission track data from the Mekong River support the Ar-Ar and U-Pb ages in favoring tectonically driven rock uplift and gorge incision as the dominant control on erosion, with precipitation being an important secondary influence.

Components: 24,746 words, 14 figures, 3 tables.

Keywords: erosion; Tibet; geochemistry; thermochronology; provenance.

Index Terms: 1130 Geochronology: Geomorphological geochronology; 8175 Tectonophysics: Tectonics and landscape evolution; 9320 Geographic Location: Asia.

Received 14 April 2006; **Revised** 19 July 2006; **Accepted** 28 July 2006; **Published** 7 October 2006.

Clift, P. D., A. Carter, I. H. Campbell, M. S. Pringle, N. Van Lap, C. M. Allen, K. V. Hodges, and M. T. Tan (2006), Thermochronology of mineral grains in the Red and Mekong Rivers, Vietnam: Provenance and exhumation implications for Southeast Asia, *Geochem. Geophys. Geosyst.*, *7*, Q10005, doi:10.1029/2006GC001336.

1. Introduction

[2] Erosion of the continental crust is controlled by the interaction of a number of processes, including tectonically driven rock and surface uplift, glaciation, precipitation, climatic seasonality, vegetation and sea level variations. Determining which of these factors, if any, is dominant over different durations of geological time is a research goal for geomorphologists, tectonicists and sedimentary geologists. In this study we have addressed this issue with a study of the erosional systems in the modern Red (Song Hong) and Mekong River systems that span much of eastern Tibet, southwest China and Indochina (Figure 1). We have employed a series of radiometric thermochrometers to constrain the source of the sandy sediment now found close to the mouths of the Mekong and Red Rivers in order to determine where this sediment is originating. These rivers are suitable targets to pursue such studies because these drainage basins span regions of varying climate and tectonic activity that should allow the dominant processes controlling erosion to be determined.

[3] Study of the thermochronology of the grains in sediment reaching these deltas allows us to resolve whether there are geochemically distinctive source regions within the drainages that might be resolved in ancient sedimentary sequences. A complete clastic sedimentary record could, in principle, be used to reconstruct ancient patterns and rates of erosion, but this is critically dependent on having the right provenance tools at our disposal. This is a particularly important issue in eastern Asia because of hypotheses proposing that large-scale capture of headwater drainage has occurred between the major rivers of the region [e.g., *Brookfield*, 1998; *Clark et al.*, 2004]. Because such capture events must affect the composition of sediment reaching each delta it should be possible to identify capture events in the sedimentary record using provenance tools. The timing of capture is proposed to be linked to the enigmatic timing of Tibetan surface uplift and is thus of wide tectonic significance. In this study we attempt to pin point which methods might be most effective at distinguishing the sources of the modern Red and Mekong Rivers in order to assess whether capture between these neighbors can be resolved in the geological record.

[4] In this study we sampled medium-grained sand from the active channels of the Red and Mekong rivers close to their present mouths and used single grain U-Pb dating of zircons, $^{40}Ar/^{39}Ar$ dating of muscovite grains, and both apatite and zircon fission track methods to identify differences between the drainage systems. We then compare these data with similar measurements from the source regions in order to determine where the sediment is now being produced, and by extension what can be said of the present state of the sources from the sediment now reaching the ocean. If an accurate picture

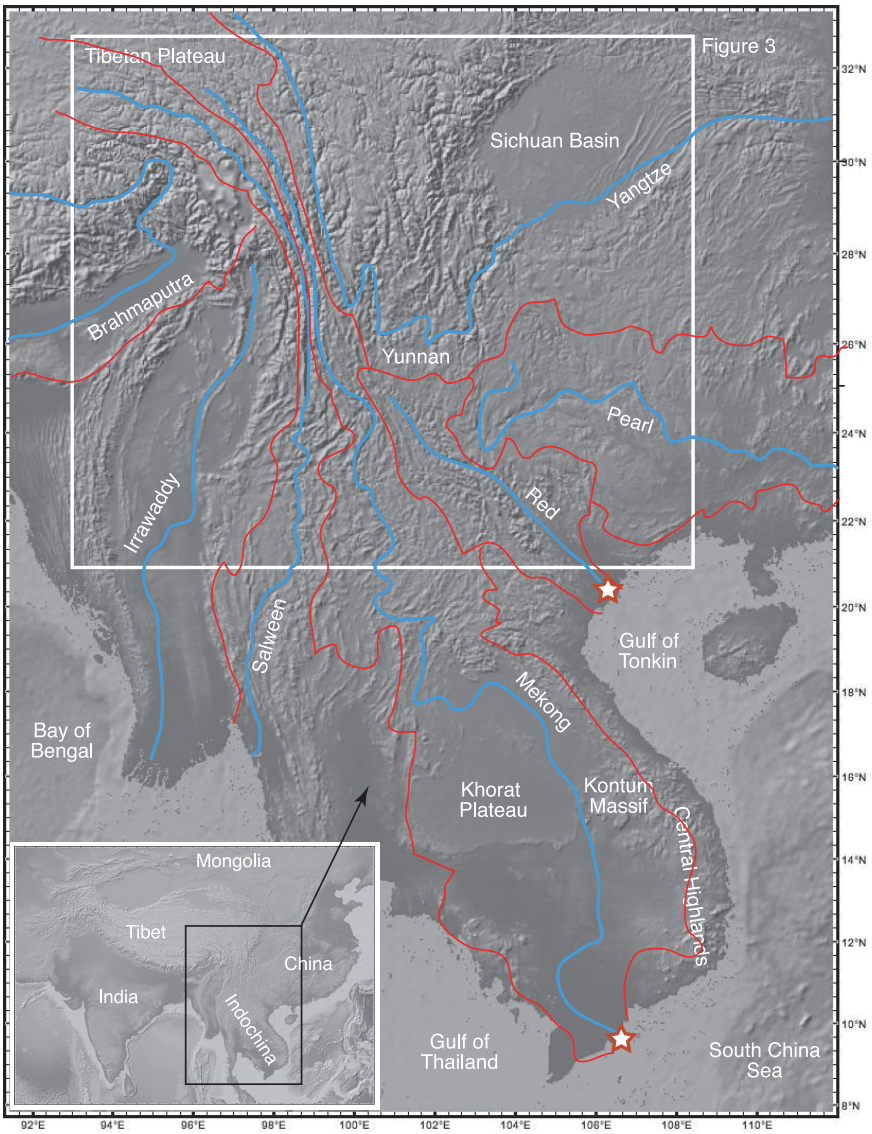

Figure 1. Shaded topographic relief map showing the study area, the major topographic features, the courses of the main rivers (blue lines), and the extent of the drainage basins (red lines) that form the focus of this study and their neighbors from whom drainage capture has been proposed. Stars mark the sampling locations for the sediments analyzed in this study. Inset shows location of Indochina within the broader context of the Himalaya-Tibetan orogen.

of the modern orogen can be reconstructed from these sediments then the same methods may prove effective in application to older sedimentary deposits.

2. Geological Setting

[5] Both the Mekong and Red rivers flow into the South China Sea (East Sea of Vietnam) after flowing from sources in the eastern Tibetan Plateau (Figures 1 and 2). The two river basins are quite different from one another in terms of their size and topography. The Mekong rises high on the Tibetan Plateau and subsequently flows over broad regions of relatively flat lying Indochina before reaching its delta. In contrast, the Red River rises in Yunnan in southwest China and follows the trace of the major strike-slip Red River Fault Zone before crossing the Hanoi Basin and developing a delta in the Gulf of Tonkin. The Red River is believed to have experienced large-scale loss of drainage due to capture into the neighboring systems [*Clark et al.*, 2004], and simple mass balance confirms that there is far more sediment preserved offshore than has been eroded in the modern catchment [*Clift et al.*, 2004a].

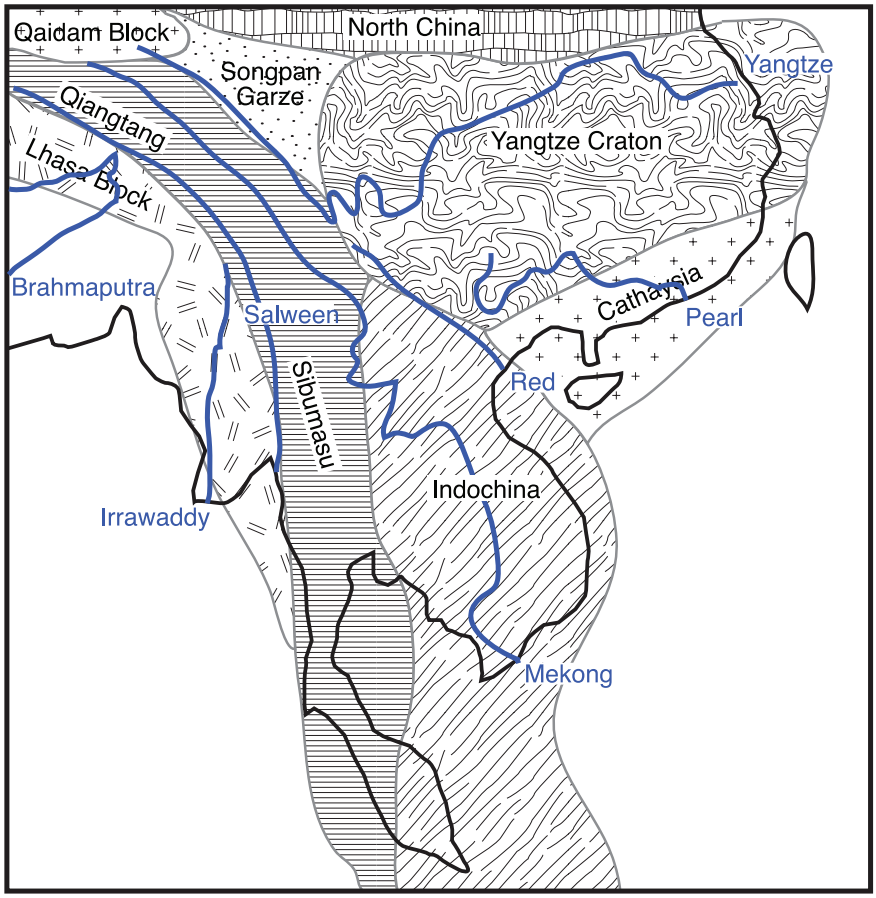

Figure 2. Simplified tectonic terrane map of East and Southeast Asia showing the major blocks discussed in this paper [after *Metcalfe*, 1996] and the courses of the rivers colored in blue.

[6] The Mekong has potentially several more sources from which to draw sediment than the Red River because of its much greater length. The bedrock geology of the region is divided into a number of terranes shown in Figure 2, with a simplified geological map (Figure 3) outlining which tectonic blocks might be providing sand to each drainage system. Close to its origin the Mekong is eroding gorges into the relatively flat surface of the Tibetan Plateau, which has been described as a pre-uplift peneplain, potentially dating back to the Eocene [*Clark et al.*, 2004]. The basement in this region is the Qiangtang Block, a continental fragment that collided with the Yangtze Craton to the north during the Triassic [*Kroener et al.*, 1993; *Grimmer et al.*, 2002, 2003]. The Qiangtang and Yangtze blocks are separated by the accreted Yidun Arc terrane [*Reid et al.*, 2005] and the Songpan Garze terrane, a Triassic accretionary complex composed largely of deformed and lightly metamorphosed turbidites eroded from the collisional Qinling-Dabie orogen formed by Yangtze-Qiangtang collision, and incorporating material from both terranes [*Bruguier et al.*, 1997; *Huang et al.*, 2003; *Roger et al.*, 2004; *Weislogel et al.*, 2006]. The Qiangtang Block is separated from South Tibet (Lhasa Block) by the Bangong-Nujiang Suture, which was open until Early Jurassic times [*Yin et al.*, 1988; *Kapp et al.*, 2003]. The Lhasa Block is another continental fragment, but is not considered a likely source of sediment to either river system because it presently lies west of the modern drainages.

[7] The Yangtze Craton is the oldest fragment of continental crust in eastern Asia and has experienced a series of collisions with its neighbors to form modern China [*Zheng et al.*, 2006]. Collision with Cathaysia to the south occurred around 1000 Ma [*Li et al.*, 2001], but this terrane remained intermittently tectonically active for a long time; last being an active continental arc in the Cretaceous before falling inactive prior to rifting of the South China Sea in the Oligocene [*Jahn et al.*, 1976]. Although this terrane dominates the Pearl River basin it is not expected to be a significant source of sediment to the Red River.

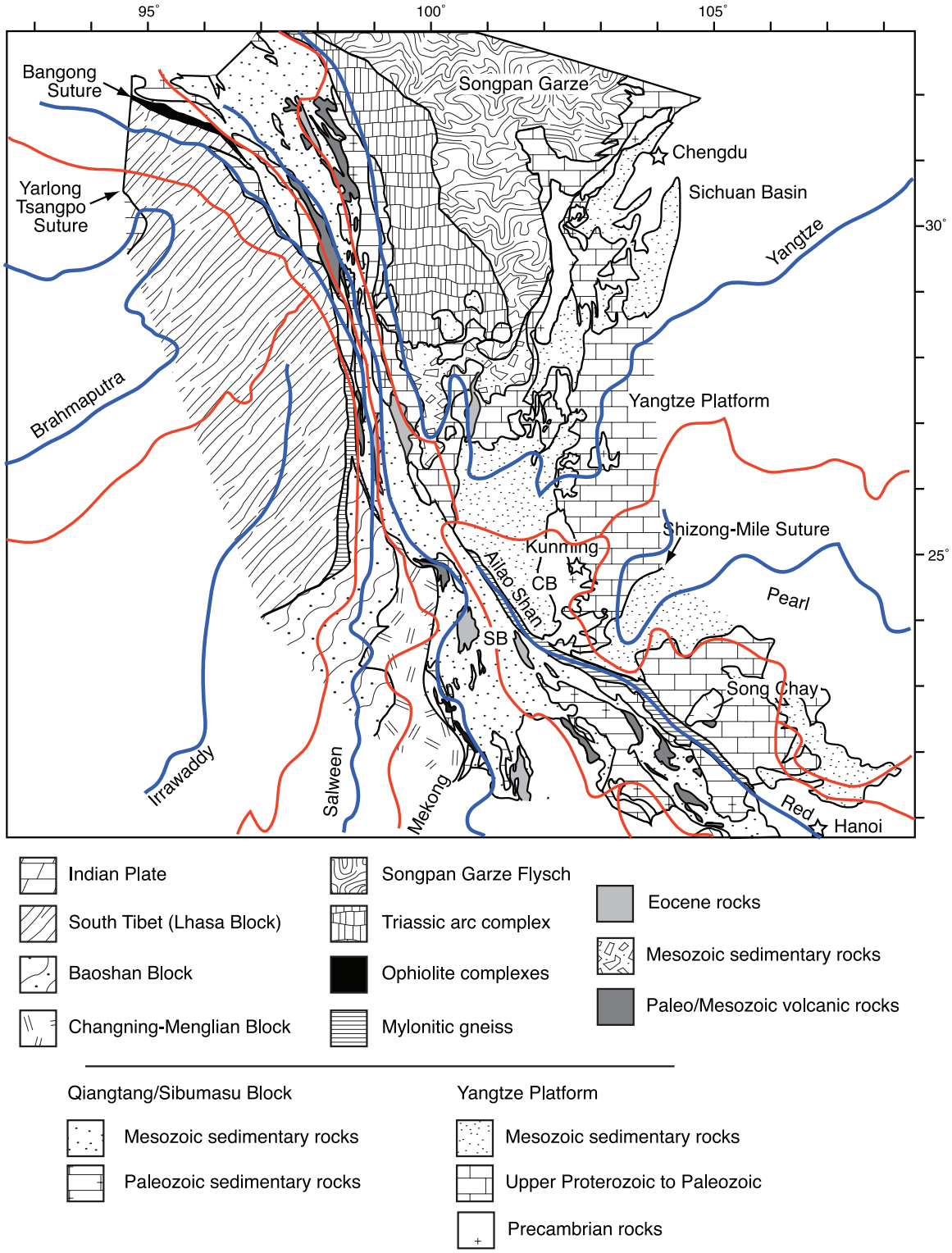

Figure 3. Regional geological map of the eastern Tibetan Plateau, SW China, and northern Indochina showing the river courses overlain in blue and the extent of the drainage basins in red. Map redrawn from original provided by B. C. Burchfiel (unpublished data, 2006). CB, Chuxiong Basin; SB, Simao Basin.

[8] To the southwest this assemblage of terranes has collided with more continental blocks in Indochina, specifically the Baoshan, Changning-Menglian and Sibumasu Blocks. This collision forms the Indosinian orogeny during the Late Triassic [e.g., *Lepvrier et al.*, 1997; *Hall*, 2002]. The Indosinian suture is partially exploited by the Cenozoic Red River Fault Zone [e.g., *Harrison et al.*, 1996; *Leloup et al.*, 2001; *Gilley et al.*, 2003], which in turn is the location of the Red River itself. As a result there is a broad geological distinction between the source rocks exposed north and east of the Red River that are dominated by the Yangtze Craton and those to the south and west, which are associated with the Baoshan and Changning-Menglian Blocks, as well as the Sibumasu Block, generally interpreted to be the southeast extension of the Qiangtang Block [*Metcalfe*, 1996].

[9] The basement of Indochina itself appears to have been widely affected by the Triassic Indosinian orogeny [e.g., *Lo et al.*, 1999; *Carter et al.*, 2001; *Nagy et al.*, 2001]. Subsequent tectonic activity formed a Triassic-Cretaceous sedimentary basin that was then inverted in the Late Cretaceous to create the Khorat Plateau of central Indochina [*Racey et al.*, 1996] (Figure 1). The whole of Indochina appears to have been transported to the southeast relative to central Asia following the collision of India and Eurasia, although the degree and timing of motion is still hotly contested [e.g., *Leloup et al.*, 2001; *Morley*, 2002; *Replumaz and Tapponnier*, 2003; *Searle*, 2006]. What is clear is that large-scale strike-slip faulting has opened up basins in Indochina and neighboring marine areas [*Morley*, 2002]. Most recently southern Vietnam has been affected by basaltic volcanism [*Flower et al.*, 1998] and associated uplift and exhumation of the Central Highlands of Vietnam after ~10 Ma [*Carter et al.*, 2000]. *Clift et al.* [2004a] calculated that if the exhumation of the Central Highlands is mostly driven by erosion and not tectonic unroofing this would be major source of sediment to the Mekong delta since the Late Miocene.

3. Basis of Provenance Methods

[10] The provenance identification methods we employ here are based on the contrasting geological histories of the various possible source regions. Sr, Nd and Pb isotopes have shown that there are major differences in petrogenesis and the age of crustal blocks in eastern Asia [e.g., *Gilder et al.*, 1996; *Ma et al.*, 2000; *Bodet and Schärer*, 2001], yet application of the Nd isotopic system to understanding sediment generation is limited because sands from the two rivers have $^{143}Nd/^{144}Nd$ ratios that are close together (0.512118 in the Mekong and 0.512047 in the Red River [*Clift et al.*, 2006]) and without details of the isotopic composition of the tributaries it is not possible to unmix these bulk sediment compositions to determine the ultimate source of the sand. Bulk sediment analytical methods are also flawed because they necessarily average the composition and do not allow end-members or minority populations to be identified.

[11] Here we employ a series of single grain measurements in order to identify specific source regions and thus quantify their relative contribution to the total sediment flux. We focus on single grain U-Pb dating of zircons, $^{40}Ar/^{39}Ar$ dating of muscovite grains and both apatite and zircon fission track methods because they have an established track record in provenance studies in Asia, as well as further afield [e.g., *Corrigan and Crowley*, 1990; *Carter and Moss*, 1999; *Carter and Bristow*, 2003; *Clift et al.*, 2004b; *DeCelles et al.*, 2004; *Campbell et al.*, 2005]. Each method identifies closure times of a different temperature range and therefore different stages of source thermal evolution, which makes their combination a powerful approach to understanding progressive source exhumation. The high temperature U-Pb data record zircon crystallization ages (~750°C), while $^{39}Ar/^{40}Ar$ dating of mica grains records post-metamorphic cooling (~350°C) and exhumation through intermediate depths and temperatures. Finally lower temperature apatite and zircon fission track ages are used to monitor exhumation and cooling in the uppermost part of the crust. An additional benefit of using different thermochronometers is that it enables a more complete picture of the sediment source to be developed and reduces lithological bias associated with the use of a single mineral phase.

[12] Zircon U-Pb dating reflects the time of zircon growth, which in most cases is the rock crystallization age. An advantage of the U-Pb system in zircon is that it has a high closure temperature and is mostly unaffected by high-grade metamorphism to temperatures at least as high as 750°C [*Cherniak and Watson*, 2001; *Carter and Bristow*, 2000]. Detrital zircon U-Pb ages from river sediments should therefore be representative of the range of crustal anatexis events within the drainage basin. However, an important disadvantage of the high closure temperature of U-Pb in zircon is that the system is not set during normal sedimentary pro-

cesses, which makes it difficult to distinguish first-cycle from multicycle grains [*Campbell et al.*, 2005]. In contrast, the $^{39}Ar/^{40}Ar$ age of a detrital mica typically reflects the time at which that mineral cooled through the 250–350°C isotherm for biotite, 350–400°C for muscovite [*Hodges*, 2003] following peak metamorphism. The technique has proven useful in dating metamorphic events throughout the Himalaya, Tibetan Plateau and East Asia. The $^{40}Ar/^{39}Ar$ method has also been successfully used as a provenance tool for dating the foreland sediments [*Najman et al.*, 2002; *White et al.*, 2002]. The low-temperature fission track method, which records cooling through ~125–60°C over timescales of 1–10 Myr in apatite [*Green et al.*, 1989], and 200–320°C in zircon [*Tagami et al.*, 1998] is particularly sensitive to exhumation driven by erosion and has been widely used in orogenic exhumation studies. It is also an effective provenance tool [e.g., *Carter*, 1999] and has been used in previous studies in the Arabian Sea [*Clift et al.*, 2004b] and Bay of Bengal [*Corrigan and Crowley*, 1990].

4. Analytical Methods

4.1. U-Pb Dating of Zircons

[13] U-Th-Pb isotopic compositions of zircons were analyzed at the Australian National University, Canberra, using Excimer Laser Ablation Inductively Coupled Plasma Mass Spectrometry (ELA-ICP-MS) employing a pulsed 193 μm ArF LambdaPhysik LPX 1201 UV Excimer laser and an Agilent 7500 quadrupole ICP-MS. The zircons were separated from the bulk sediment by conventional magnetic and heavy liquid separation techniques. The extracted zircons were mounted in epoxy resin and polished. Dating by ELA-ICP-MS followed the procedure described by *Campbell et al.* [2005]. Our method employs standard zircon TEMORA2 and NIST610 silicate glass [*Pearce et al.*, 1997; *Black et al.*, 2004] where the latter is used for concentration information and for U/Th determination. As we cannot measure common Pb (^{204}Pb) directly because of systemic Hg, we use a ^{208}Pb-based correction *only* when that correction makes the analysis more concordant than the uncorrected version. Once the data were compiled, an analysis was rejected for interpretation on the basis of the following: (1) the observed variance on $^{206}Pb/^{238}U$ or $^{207}Pb/^{206}Pb$ (depending if the grain is > or <1200 Ma) is more than three times that calculated from counting statistics (this procedure omits grains that record mixed ages), or (2) the grain is deemed to be discordant. Analysis time drift corrections were applied to both analytical sessions. R33 returned ages one percent below the TIMS age (419.26 ± 0.39 Ma [*Black et al.*, 2004]) for both analytical days. On 20 July 2005, 19 of 19 grains of R33 gave 414.7 ± 2.5 Ma with mean weighted standard deviation (MSWD) = 1.81. On 29 August 2005 18 of 18 grains yielded 414.9 ± 3.1 Ma with an MSWD of 1.25. This means that quoted $^{206}Pb/^{238}U$ ages may be one percent low when compared to other techniques. $^{207}Pb/^{206}Pb$ ages appear accurate.

[14] Results of the U-Pb dating are shown in Table 1. Quoted 1 s.e. uncertainties on individual grains include a term for that particular ablation in quadrature with a term that reflects our ability to measure the standard zircon. Overall uncertainty on an individual measurement is about 1–2%. This method of error propagation produces reasonable MSWDs on secondary standards known to comprise a single age population, in this case zircon standard R33 [*Black et al.*, 2004].

4.2. $^{40}Ar/^{39}Ar$ Analysis of Mica Grains

[15] Single crystal $^{40}Ar/^{39}Ar$ laser-fusion analyses were performed at the Massachusetts Institute of Technology (MIT). Prior to analysis, samples were irradiated in the C5 position of the McMaster University Nuclear Reactor, Canada, using 1 mm Cd shielding for 4 hours at a power level of 2 MW. After fusion with an Ar-ion laser, the released gases were purified for 10 min with two Al-Zr getters operated at 400 deg C and room temperature, respectively, and then admitted to an MAP 215-50 mass spectrometer for Ar isotopic analysis using a Johnson MM-1 electronic multiplier operated at a gain of about 10,000. The conversion efficiency of ^{39}K to ^{39}Ar was monitored using sanidine from the Taylor Creek rhyolite (TCR-2a) assuming an age of 28.34 Ma [*Renne et al.*, 1998], and is known to better than 0.3% (1 standard deviation). Corrections for neutron-induced interferences, determined using Fe-doped kalsilite glass and optical CaF_2, were 0.00039 for $^{40}Ar/^{39}Ar_K$, 0.01243 for $^{38}Ar/^{39}Ar_K$, 0.000672 for $^{39}Ar/^{37}Ar_{Ca}$, 0.000033 for $^{38}Ar/^{37}Ar_{Ca}$, and 0.00028 for $^{36}Ar/^{37}Ar_{Ca}$. Final data reduction was conducted with the program ArArCalc [*Koppers*, 2002]; results are shown in Table 2.

4.3. Fission Track Analysis

[16] Apatite and zircon fission track analysis was performed at University College, London, UK.

Table 1 (Representative Sample). Analytical Data for Mekong and Red River Sands From ICP-MS Laser Analysis of Zircon Grains for U-Pb Geochronology[a] [The full Table 1 is available in the HTML version of this article at http://www.g-cubed.org]

Grain Number	Pb*, ppm	U, ppm	Atomic Th/U	Uncorrected $^{206}Pb/^{238}U$ Ratio	± s.e.	Uncorrected $^{207}Pb/^{235}U$ Ratio	± s.e.	Uncorrected $^{207}Pb/^{206}Pb$ Ratio	± s.e.	Uncorrected $^{208}Pb/^{232}Th$ Ratio	± s.e.	% Common ^{206}Pb Using ^{208}Pb	% Common ^{206}Pb Using ^{207}Pb
Red River													
1	62.14	271.89	0.42748	0.21747	0.00155	2.95226	0.04119	0.09846	0.00118	0.06921	0.00151	0.419	1.932
2	80.46	525.57	0.10631	0.15992	0.00061	1.53155	0.01322	0.06946	0.00054	0.05057	0.00052	0.052	−0.183
3	89.37	1159.94	0.81977	0.06778	0.00042	0.49978	0.00640	0.05348	0.00060	0.01997	0.00017	−0.754	−0.217
4	107.31	852.95	0.30962	0.12465	0.00045	1.14942	0.00885	0.06688	0.00045	0.04087	0.00025	0.333	0.293
5	79.49	143.56	0.66177	0.47220	0.00172	10.50206	0.06184	0.16130	0.00075	0.12884	0.00092	−0.159	−0.328
6	25.82	178.11	0.89911	0.12417	0.00075	1.09238	0.01693	0.06381	0.00091	0.03749	0.00043	−0.280	−0.071
7	7.61	272.04	0.48265	0.02675	0.00017	0.17526	0.00489	0.04751	0.00129	0.00846	0.00014	0.009	−0.240
8	50.76	589.30	0.60450	0.07951	0.00031	0.60752	0.00677	0.05542	0.00058	0.02449	0.00016	−0.071	−0.198
9	148.04	476.31	0.09459	0.31628	0.00105	5.06846	0.02553	0.11622	0.00044	0.09304	0.00096	0.010	1.004
10	60.92	168.87	0.49749	0.33041	0.00133	5.07201	0.03974	0.11133	0.00075	0.09435	0.00061	−0.069	−0.149
11	76.70	2083.45	0.14551	0.03871	0.00036	0.27282	0.00616	0.05111	0.00105	0.01215	0.00023	−0.007	0.002
12	46.39	679.99	0.24707	0.06916	0.00041	0.53367	0.00679	0.05597	0.00063	0.02349	0.00053	0.307	0.061
13	78.11	701.94	0.68823	0.09804	0.00062	0.93902	0.01396	0.06947	0.00094	0.03956	0.00050	3.601	1.171
14	68.20	177.75	0.72576	0.33796	0.00253	7.24231	0.06726	0.15542	0.00085	0.09848	0.00081	0.121	5.397
15	8.83	146.26	1.09805	0.04964	0.00030	0.35443	0.01195	0.05178	0.00172	0.01523	0.00017	−0.361	−0.102
16	131.76	1473.62	0.56865	0.08356	0.00024	0.65273	0.00464	0.05666	0.00037	0.02472	0.00013	−0.415	−0.123
17	366.49	817.03	0.64293	0.39329	0.00219	9.11136	0.06328	0.16802	0.00070	0.12885	0.00100	1.335	4.797
18	4.30	108.38	0.56119	0.03735	0.00033	0.28749	0.00969	0.05582	0.00181	0.01137	0.00020	−0.275	0.606
19	4.83	116.97	0.52908	0.03904	0.00034	0.27274	0.00950	0.05067	0.00171	0.01219	0.00024	−0.022	−0.057
20	312.74	862.21	0.39585	0.34279	0.00101	6.95375	0.03201	0.14713	0.00052	0.09928	0.00067	0.037	4.065
21	40.21	303.21	0.55270	0.12372	0.00055	1.08007	0.01211	0.06332	0.00065	0.03709	0.00029	−0.179	−0.121
22	190.32	489.61	0.62457	0.34528	0.00157	5.74057	0.03504	0.12058	0.00049	0.09814	0.00070	−0.093	0.451
23	43.22	558.23	0.66094	0.07042	0.00028	0.55600	0.00604	0.05726	0.00058	0.02227	0.00016	0.165	0.196
24	14.90	187.07	1.03813	0.06633	0.00033	0.51393	0.00955	0.05620	0.00101	0.02044	0.00018	−0.180	0.141
25	104.34	575.91	0.16335	0.18604	0.00064	1.98199	0.01371	0.07727	0.00046	0.05322	0.00092	−0.051	0.132
26	174.11	523.04	0.26078	0.32353	0.00112	5.08981	0.02610	0.11410	0.00043	0.09557	0.00061	0.076	0.463
27	135.15	2668.13	1.18647	0.04086	0.00017	0.30992	0.00305	0.05500	0.00049	0.01260	0.00006	−0.435	0.445
28	84.66	181.14	0.74137	0.40159	0.00158	7.74742	0.05857	0.13992	0.00090	0.10561	0.00129	−0.803	0.527
30	388.89	980.25	0.73126	0.34705	0.00275	6.30042	0.06041	0.13167	0.00071	0.09313	0.00070	−0.656	1.821
31	40.52	234.42	1.91440	0.11983	0.00052	1.30421	0.01696	0.07894	0.00097	0.03810	0.00023	1.418	1.898
32	43.84	126.12	0.78937	0.29984	0.00104	4.31243	0.03606	0.10431	0.00079	0.08561	0.00059	−0.206	0.083
33	69.33	1293.25	1.48776	0.04034	0.00014	0.29790	0.00332	0.05356	0.00057	0.01274	0.00007	0.126	0.276
34	66.76	500.41	0.65947	0.12124	0.00063	1.06247	0.01428	0.06356	0.00079	0.03638	0.00030	−0.226	−0.040
35	44.15	625.24	0.44628	0.06802	0.00027	0.51340	0.00567	0.05474	0.00056	0.02102	0.00017	−0.063	−0.068
36	67.44	721.87	0.30855	0.09325	0.00045	0.77343	0.01305	0.06016	0.00097	0.02858	0.00043	−0.051	0.116

[a] Abbreviations: yu, younger than 900 Ma and no common Pb correction; yc, younger than 900 Ma and ^{208}Pb-based common Pb correction; ou, older than 900 Ma and no common Pb correction; oc, older than 900 Ma and ^{208}Pb-based common Pb correction.

Table 2. Analytical Data From $^{39}Ar/^{40}Ar$ Analysis of Muscovite Grains From the Mekong and Red Rivers

Age, Ma	±2s	$^{40}Ar(r)$, %	$^{39}Ar(k)$, %
		Mekong River	
22.37	±0.36	95.56	7.47
22.84	±1.10	95.65	2.41
24.85	±1.71	93.56	1.53
25.63	±2.29	94.90	1.07
26.60	±1.76	93.27	1.37
28.37	±0.77	98.14	3.38
28.71	±1.81	91.14	1.36
28.89	±1.70	91.11	1.51
29.84	±0.69	94.41	3.71
29.93	±2.01	87.58	1.26
80.47	±1.65	98.27	1.89
83.95	±0.73	98.12	5.93
105.13	±1.75	98.30	2.04
143.96	±1.83	98.61	2.38
155.55	±3.83	98.64	1.36
158.07	±2.47	98.13	1.90
161.49	±1.85	98.81	2.69
167.33	±2.63	98.28	1.83
168.31	±4.07	94.96	1.16
171.12	±2.82	96.62	1.74
171.86	±4.27	96.73	1.12
173.48	±3.21	98.21	1.64
177.53	±3.47	98.39	1.40
177.68	±2.11	99.11	2.61
180.87	±3.82	95.48	1.25
181.05	±4.12	96.15	1.49
181.68	±5.30	98.43	0.91
183.69	±1.99	98.92	3.02
183.73	±2.08	98.95	3.32
187.64	±4.51	97.35	1.11
187.68	±3.18	94.92	1.66
189.33	±2.11	98.97	2.83
190.79	±3.04	98.85	2.01
192.58	±2.62	98.36	2.01
193.20	±3.93	98.51	1.54
195.43	±3.55	99.26	1.42
195.73	±3.18	98.52	1.77
197.16	±2.15	97.98	2.75
198.29	±2.92	98.80	2.21
199.94	±3.31	98.48	1.81
200.55	±3.23	99.11	2.08
201.84	±2.83	98.32	1.96
202.07	±3.73	95.68	1.61
206.14	±3.10	98.80	1.85
206.76	±4.65	97.63	1.15
207.61	±3.43	98.05	1.84
210.63	±2.55	99.13	2.73
215.12	±7.46	99.30	0.89
		Red River	
17.06	±0.44	94.73	5.07
17.14	±0.66	89.41	3.19
17.69	±1.08	85.05	2.00
17.82	±1.21	77.69	1.73
17.95	±0.90	93.69	2.35
18.00	±0.35	93.82	6.26
18.13	±0.39	87.49	5.46
20.12	±1.93	88.17	1.12
20.58	±0.72	90.13	2.96
20.84	±0.31	80.44	8.77
21.10	±0.80	93.25	2.69
30.48	±1.01	90.47	2.12
50.10	±0.66	97.96	3.69
194.57	±2.25	99.07	2.26
202.45	±2.12	98.64	2.44
202.95	±2.88	97.40	1.82
206.21	±3.12	98.53	1.59
206.26	±2.42	98.21	2.00
209.54	±2.54	99.07	2.22
223.08	±3.21	99.11	1.94
224.68	±3.33	97.29	1.64
226.31	±3.64	98.84	1.48
226.36	±4.38	97.94	1.19
227.01	±3.18	98.60	1.63
227.32	±3.36	98.08	1.62
228.50	±2.93	97.54	1.96
228.56	±3.64	97.99	1.40
228.78	±2.49	99.33	2.19
229.18	±4.40	97.75	1.24
229.78	±2.39	99.39	2.27
229.88	±4.62	96.51	1.14
230.44	±4.17	99.35	1.35
231.74	±2.63	99.18	2.16
233.05	±3.79	97.72	1.44
233.35	±4.67	96.90	1.11
235.53	±3.83	95.94	1.51
236.98	±3.53	99.14	1.57
245.88	±3.28	94.77	1.73
248.83	±3.67	99.59	1.65
327.75	±8.22	98.23	0.81
333.50	±5.73	98.73	1.29
350.59	±6.32	98.53	1.18
369.63	±10.91	98.43	0.82
379.64	±10.87	98.35	0.80
384.54	±8.53	98.85	1.05
398.83	±7.95	98.56	1.10
404.05	±7.95	96.76	1.02

Polished grain mounts were etched with 5N HNO_3 at 20°C for 20 seconds s to reveal the spontaneous fission tracks. Subsequently the uranium content of each crystal was determined by irradiation, which induced fission of ^{235}U. The induced tracks were registered in external mica detectors. The samples for this study were irradiated in the thermal facility of the Hifar Reactor at Lucas Heights, Australia. The neutron flux was monitored by including Corning glass dosimeter CN-5, with a known uranium content of 11 ppm, at either end of the sample stack. After irradiation, sample and dosimeter mica detectors were etched in 48% HF at 20°C for 45 min. Only crystals with sections parallel to the c-crystallographic axis were counted, as these crystals have the lowest bulk etch rate. To avoid biased results through preferred selection of apatite crystals the sample was systematically scanned and each crystal encountered with the correct orienta-

Table 3. Fission Track Analytical Data for Mekong and Red River Sediment[a]

Sample Number/ Field Number	Mineral	Number of Crystals	Dosimeter		Spontaneous		Induced		Age Dispersion		Central Age, Ma, ±1σ	1st Age Comp.	2nd Age Comp.	3rd Age Comp.	4th Age Comp.	5th Age Comp.
			ρd	Nd	ρs	Ns	ρi	Ni	$P\chi^2$	RE%						
Mekong River	Apatite	19	1.317	3651	0.798	403	5.340	2697	0	60.9	39.6 ± 6.4	14.6 ± 1.9(7)	27.1 ± 4.1(6)	66.2 ± 6.4(6)		
	Zircon	45	0.606	6715	8.480	7781	3.437	3154	0	79.2	100.3 ± 12.1	22.2 ± 1.2(5)	45.3 ± 4.7(4)	68.9 ± 3.7(10)	147.8 ± 7.3(15)	147.8 ± 7.3(15)
Red River	Apatite	67	1.00	2762	0.279	1461	2.124	11142	0	55.3	23.1 ± 1.8	4.4 ± 0.9 (6)	14.9 ± 2.3 (14)	20.5 ± 1.4 (38)	32.5 ± 3.7 (6)	75.1 ± 6.9 (4)
	Zircon	40	0.426	2921	9.948	9665	3.493	3394	0	75.1	78.3 ± 9.5	30.4 ± 1.1 (11)	53.9 ± 5.0 (6)	101.8 ± 6.4 (10)	199.3 ± 13.3 (12)	

[a]Notes: (1) Track densities are ($\times 10^6$ tr cm^{-2}); numbers of tracks counted (N) shown in brackets. (2) Analyses by external detector method using 0.5 for the $4\pi/2\pi$ geometry correction factor. (3) Ages calculated using dosimeter glass CN-5; (apatite) ζ_{CN5} = 338 ± 4; CN-2 (zircon) ζ_{CN2} = 127 ± 4 calibrated by multiple analyses of IUGS apatite and zircon age standards [see *Hurford*, 1990]. (4) $P\chi^2$ is probability for obtaining χ^2 value for v degrees of freedom, where v = number of crystals − 1. (5) Central age is a modal age, weighted for different precisions of individual crystals [see *Galbraith*, 1990]. (6) Data were deconvolved into component ages using the statistical approach of *Sambridge and Compston* [1994].

tion was analyzed, irrespective of track density. The chi-test was used to determine whether each sample contained a mixed population of single grain ages and if so were deconvolved into component ages using the statistical approach of *Sambridge and Compston* [1994]. Based on mixture modeling, this approach uses several competing methods to derive most likely ages, their proportions and number of distinct components. This procedure includes the binomial peak-fitting algorithm of *Galbraith and Green* [1990]. No track lengths were measured due to the low track density and insufficient grains within each age mode. The results of the fission track analysis are presented in Table 3.

5. Results of U-Pb Zircon Dating

[17] The results of the U-Pb analyses are shown graphically in Figure 4 in which the ages are shown in the form of a probability density diagram. Grain ages range from as young as 33 ± 0.3 Ma in the Red River and 73 ± 0.7 Ma in the Mekong to as old as 2469 ± 17 Ma and 2693 ± 20 Ma respectively. The vast majority of grains pre-date India-Asia collision, showing that there was little crustal anatexis within the Mekong and Red drainages as a result of that event. The two rivers share many similarities in the age structure of their populations at the first order level. Significant numbers of grains are found in the age ranges 200–300 Ma, 400–500 Ma, 1700–1800 Ma and ~2500 Ma. The Red River contrasts with the Mekong sample in showing a well-developed population dated at 700–800 Ma. At a first order level the samples appear to be eroding crust of quite similar tectonic origins, which is perhaps not surprising given the close proximity of their headwater in eastern Tibet and Yunnan (Figures 1–3). The provenance of the sediments can be partially constrained by comparing the ages seen in the river with those of possible source terrains from the area. Age probability density diagrams using existing data from source region studies are shown plotted on the same scale in Figure 4. These diagrams compile a large volume of published data and are believed to be broadly representative of the different tectonic blocks in Southeast Asia. References to the data sets used are given in the figure caption to Figure 4.

[18] Comparison of the river sediment and bedrock analyses immediately reveals some clear patterns. Cathaysia, the Mesozoic arc province of southeast China, shows a prominent age peak at ~1400 Ma that is not seen in either river sample. This is

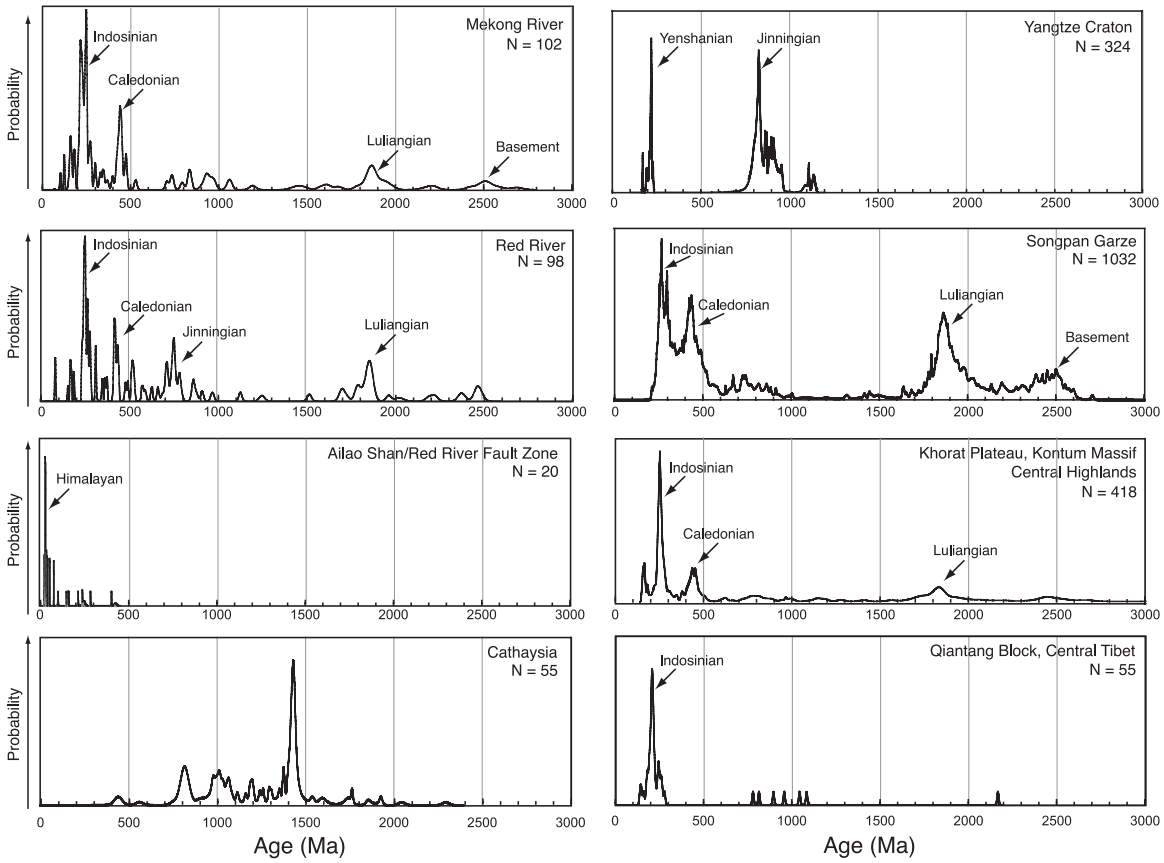

Figure 4. Age spectrum diagram for U-Pb ages measured from detrital zircons in the Red and Mekong Rivers. Diagram compares the detrital ages known from the major tectonic blocks in SE Asia. Data for Ailao Shan and Red River Fault Zone rocks are from *Schärer et al.* [1990, 1994], *Zhang and Schärer* [1999], *Nagy et al.* [2000], and *Carter et al.* [2001]. Data for Cathaysia are from *Li et al.* [1989, 2002, 2005]. Data for Indochina sources (including Khorat Plateau, the Kontum Massif, and Central Highlands of Vietnam) are from *Carter and Moss* [1999], *Carter et al.* [2001], *Nagy et al.* [2001], *Carter and Bristow* [2003], and A. Carter (unpublished data, 2006). Data for the Songpan Garze Terrane are from *Wang et al.* [2000], *Bruguier et al.* [1997] and *Weislogel et al.* [2006]. Data for the Yangtze Craton (not including the Dabie Shan) are from *Li* [1999], *Ling et al.* [2003], and *Yang et al.* [2005]. Data for the Qiantang Block are from *Roger et al.* [2000, 2003].

consistent with the fact that neither river drains that block, unlike the Pearl River. Our study shows the effectiveness of the U-Pb method in distinguishing between major tectonic terranes in Southeast Asia. High-grade metamorphic rocks from within the Cenozoic shear zones of the Red River Fault Zone have been largely dated in the range 20–35 Ma [e.g., *Leloup et al.*, 2001; *Gilley et al.*, 2003], which is not present in the Mekong and is only seen in two grains from the Red River. This indicates that the high-grade rocks of the Cenozoic shear zones cannot be major contributors to either river's load, despite the great depths from which they have been exhumed in the relatively recent geological past.

[19] Comparison of the river sediment data with U-Pb ages from the Yangtze Craton is complicated because the most extensive studies of this unit have been made in the Qinling Shan-Dabie Shan orogen in northeast China, far from the drainages we discuss here and where the Yangtze Craton has been involved in collision with the North China Block [*Kroener et al.*, 1993; *Grimmer et al.*, 2002, 2003; *Hacker et al.*, 1998, 2000]. In this context comparison may not be appropriate and thus we focus on ages taken from studies of the southern Yangtze Craton, specifically from the work of *Li* [1999], *Ling et al.* [2003], and *Yang et al.* [2005]. Figure 4 shows that the southern Yangtze Craton is characterized by dates of 200–250 Ma and 800–1000 Ma, named the Yenshanian and Jinningian Events [*Chen and Jahn*, 1998; *Li*, 1999; *Chen et al.*, 2001], associated with the Indosinian Orogeny and the break-up of Rodinia respectively. These two age populations are seen clearly in the Red

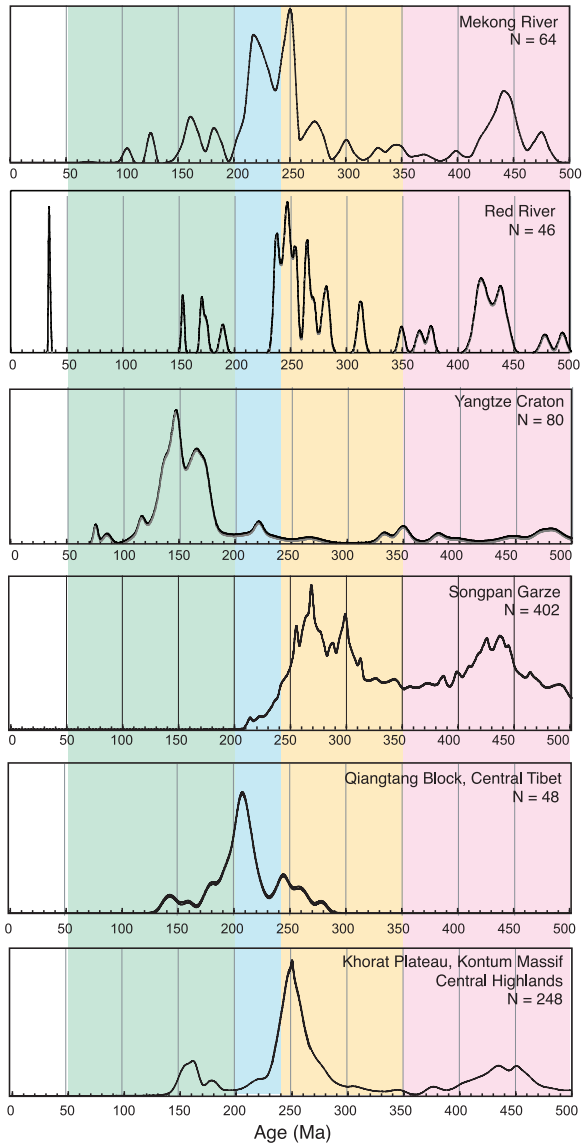

Figure 5. Age spectrum diagram for U-Pb ages measured from detrital zircons in the Red and Mekong Rivers, with only the most recent 500 Ma shown. Data sources are listed in caption for Figure 3. Colored bands highlight age range of grains related to specific tectonomagmatic events and thus possible source regions. Light green, Yenshanian; yellow, Indosinian from Qiangtang Block; light blue, Indosinian from Indochina; light orange, Caledonian from Yangtze Craton.

River sediment but the 800–1000 Ma population is less well developed in the Mekong. This pattern suggests that the Red River is preferentially eroding rocks derived from the Yangtze Craton, or its deformed margins. Given the modern drainage patterns, with the Yangtze Craton and its cover exposed northeast of the Red River Fault Zone this is an expected result.

[20] We also compare the river sediments with the rocks of the Songpan Garze terrane in Tibet despite the fact that this unit lies outside both drainages. The Songpan Garze is dominated by a deformed series of metamorphosed turbiditic sandstones and shales, interpreted as a Triassic accretionary complex [*Huang et al.*, 2003; *Weislogel et al.*, 2006], and intruded by late Triassic-early Jurassic granites [*Roger et al.*, 2004]. Because the sediment in the Songpan Garze is eroded from the Triassic Qinling-Dabie Orogen of eastern China it has the ability to sample wide areas of source terrain that are not always recognized at outcrop. The age spectrum from the Songpan Garze shows some important difference with the Yangtze Craton data. In particular, age peaks at 250–300 Ma, 400–500 Ma, and 1800–2000 Ma are recognized that correspond to a series of tectonic events in East Asia termed the Indosinian, the Caledonian, and the Luliangian, respectively [*Chen and Jahn*, 1998; *Li*, 1999; *China Geological Survey*, 2004]. An additional peak at ~2500 Ma is interpreted as reflecting the ancient basement of the Yangtze Craton [*Zheng et al.*, 2006].

[21] The 400–500 Ma, 1800–2000 Ma and 2500 Ma peaks have been recognized in both river systems as minor contributions, with slightly greater influence in the Red compared to the Mekong. The Indosinian peak is however a very major contribution to both systems, forming the largest single grain population and indicative of how important Triassic orogeny has been in reworking the crust in East Asia. Unfortunately for provenance goals the Indosinian, Caledonian and Luliangian groups have also been recognized within the basement terrains of Indochina, as exposed in the Khorat Plateau, Kontum Massif and the Central Highlands of Vietnam [*Nagy et al.*, 2001; *Carter et al.*, 2001]. Because these ages are so ubiquitous they have limited potential as decisive provenance indicators. Similarly, the limited analyses available from the Qiangtang Block of central Tibet also show a clear Indosinian peak [*Roger et al.*, 2000, 2003].

5.1. Age Differences With the Indosinian

[22] A more detailed look at possible source provenance is provided by plotting only the youngest 500 Ma of the age spectra (Figure 5). At this enlarged scale it is possible to see that the Indosinian peaks in the Red and Mekong rivers are not identical, but that the Mekong preferentially develops a peak at 210–240 Ma compared to a 230–290 Ma range in the Red River. Clearly the

Mekong is draining crust in which the Indosinian Orogen occurred earlier compared to the Red River. Comparison of this pattern with the possible source areas shows that the known ages from the southern Yangtze Craton match those in the Mekong, although this is an unlikely source given the overall patterns and the nature of the modern drainage. Instead we note that younger ages also match those found in the Qiangtang Block, which is the primary terrane exposed in the upper reaches of the Mekong River. The Sibumasu Block of Indochina is often interpreted as an equivalent of the Qiangtang Block and could be an additional source of the 210–240 Ma grains seen in the Mekong drainage.

[23] The 230–290 Ma ages seen in the Red River correspond quite well to the basement of Indochina, as measured in the Khorat Plateau, Kontum Massif and Vietnamese Central Highlands. Equivalent units are exposed southwest of the Red River Fault Zone within the Red River catchment and could be the source of these grains. It is noteworthy that although they are a small population these ages are also seen in the Mekong River, consistent with the fact that this river currently drains the Khorat Plateau in central Indochina. Not surprisingly there is no good match in detail between the river grains and the Songpan Garze Block.

5.2. Sediment Budgets

[24] By dividing up the age spectrum into a series of ranges, corresponding to tectonic events, we can make an approximate mass flow budget for the zircons that are now feeding the Red and Mekong Rivers. Here we point out that, because U-Pb in zircon cannot distinguish between first-cycle and multicycle zircons, the U-Pb dates record the age of zircon crystallization in the ultimate source of the zircons, which is not necessarily the source of the zircons in the current cycle of erosion and sedimentation [*Campbell et al.*, 2005]. We divide the population into the following classes: Himalayan (<50 Ma), Yenshanian (50–150 Ma), Late Indosinian (150–240 Ma), Early Indosinian (240–300 Ma), Caledonian (300–500 Ma), Jinningian (700–1000 Ma), Luliangian (1700–2100 Ma) and Yangtze Basement (2300–2600 Ma). As might be expected there are significant differences between the Red and Mekong rivers. The Red is distinctive in having a small Himalayan population, a much larger input from Jinningian and Luliangian sources in the Yangtze Craton and a far smaller proportion of the younger Indosinian grains. Because these younger grains are recognized in the Qiangtang Block we infer that the Mekong is deriving more of its current load from that area and its equivalents in the Sibumasu Block, while the Red River is receiving more material from the Yangtze Craton.

6. Results of Ar-Ar Mica Dating

[25] A probability density diagram displaying the $^{40}Ar/^{39}Ar$ ages for each river sediment sample is shown in Figure 6, where the spectra can be compared with each other and with those from possible source regions. The dominance of Indosinian Triassic sources to both rivers is clearly shown in this figure, although like the zircon dates the Mekong shows a consistent offset to younger ages compared with the Red River. In contrast to the U-Pb ages both sets of $^{40}Ar/^{39}Ar$ ages show a resolvable, albeit minority Himalayan-aged population. Again the age populations are offset, and again it is the Red River that gives the older ages. The Mekong also differs from the Red River in having a small number of grains in the 80–110 Ma range.

[26] $^{40}Ar/^{39}Ar$ dating of the source regions in Southeast Asia is very patchy, with large amounts of data available from the Red River Fault Zone and other regions of special tectonic character or active deformation, and very sparse data outside these areas [*Leloup et al.*, 1993, 2001; *Harrison et al.*, 1996; *Wang et al.*, 1998; *Jolivet et al.*, 1999; *Maluski et al.*, 2001]. There is a clear match between the metamorphic rocks of the Red River Fault Zone that were exhumed during the principle 34–17 Ma phase of left-lateral motion [*Gilley et al.*, 2003] and the younger (20–35 Ma) mica grains in the rivers. Even if the rocks in the Red River Fault Zone are not providing sediment to the Mekong then rocks in other similar structures, with similar deformational histories (e.g., Wang Chao Fault Zone [*Lacassin et al.*, 1997]) are providing material to that drainage. Triassic $^{40}Ar/^{39}Ar$ ages measured in the Songpan Garze and Qiangtang Blocks record the Indosinian Orogeny in those regions [*Reid et al.*, 2005; *Kapp et al.*, 2000]. Most Indosinian basement ages are older than 200 Ma, but the 150–200 Ma range that dominates the Mekong sample may also be reflected in both these blocks. Moreover, there are Cretaceous cooling ages recorded, especially in the Songpan Garze, indicating continued tectonism and magmatism after the peak of the Indosinian Orogeny. Although the modern Songpan Garze is not the source of these grains in the Mekong we infer that sources in

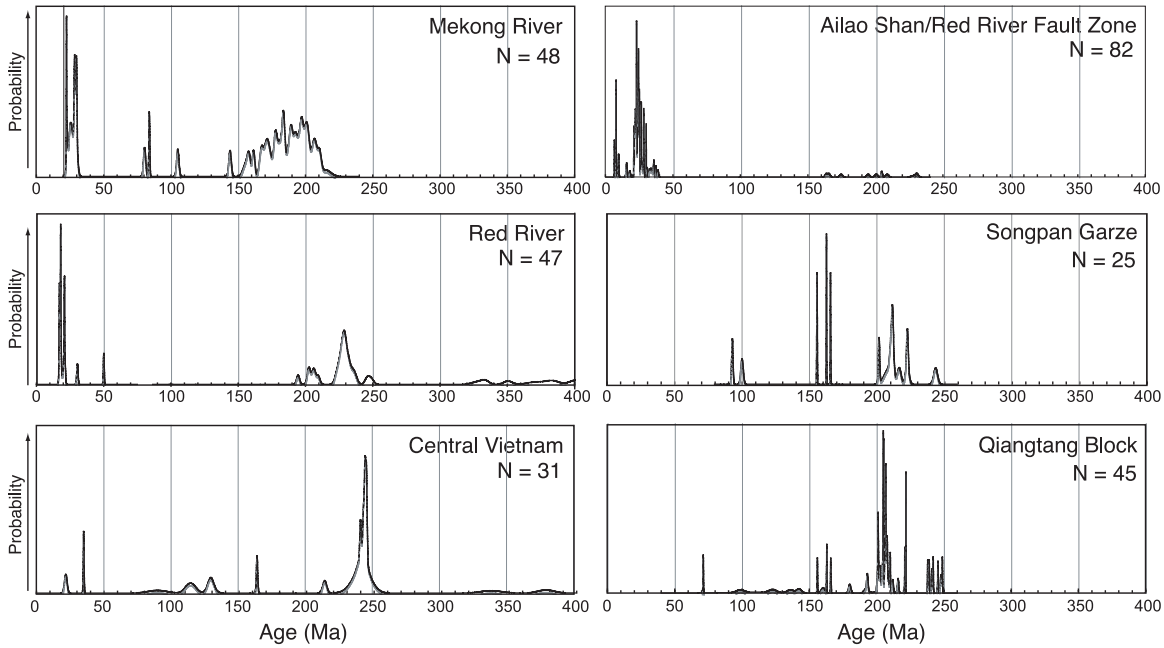

Figure 6. Probability density diagrams for Ar-Ar ages of detrital muscovites within the Mekong and Red Rivers compared to known ranges from possible source regions. Central Vietnam data are from *Lepvrier et al.* [1997] and *Nagy et al.* [2001]. Ailao Shan/Red River Fault Zone data are from *Leloup et al.* [1993, 2001], *Harrison et al.* [1996], *Wang et al.* [1998], *Jolivet et al.* [1999], and *Maluski et al.* [2001], and data from Songpan Garze are from *Reid et al.* [2005]. Qiangtang Block data are from *Kapp et al.* [2000].

Tibet that also experienced this period of active margin development would be capable of providing such material to the river, either directly, or potentially reworked through Mesozoic sedimentary rocks.

[27] As for the zircons it is possible to calculate a large-scale budget for each river on the basis of the mica cooling ages (Figure 7). In this case we divide the grains into the following categories: Himalayan (<50 Ma), Transhimalayan (50–150 Ma), Indosinian – Young (150–200 Ma), Indosinian – Old (200–250 Ma) and Caledonian (350–500 Ma). Compared to the zircons in which the differences between the drainages were more subtle, the Ar-Ar ages show a strong difference between the two basins. The Red River not only has a higher proportion of Himalayan ages grains, probably derived from the rocks in and around the Red River Fault Zone, but also has a unique population of older grains that cooled below their closure temperature (~350°C) before 350 Ma, and which are associated with Caledonian-aged events within the Yangtze Craton. In contrast, almost 75% of the Mekong drainage is dominated by sources that cooled during the Indosinian Orogeny, mostly due the later stages and/or aftermath of that event. On the basis of the mica and zircon data we infer that the dominant source of these Indosinian grains was likely the Qiangtang Block of Tibet, with some additional contribution from mainland Indochina.

7. Fission Track Results

[28] The apatite and zircon fission track results are shown graphically as radial plots in Figure 8, allow-

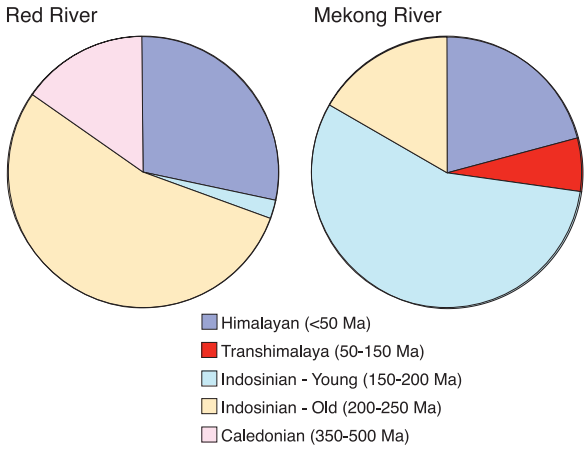

Figure 7. Pie diagram showing the contrasting origin of micas in the Red and Mekong Rivers. Himalayan grains are those <50 Ma. Transhimalaya represent cooling ages of 50–150 Ma. Indosinian ages are split into young (150–200 Ma) and old (200–350 Ma), with >350 Ma classed as Caledonian.

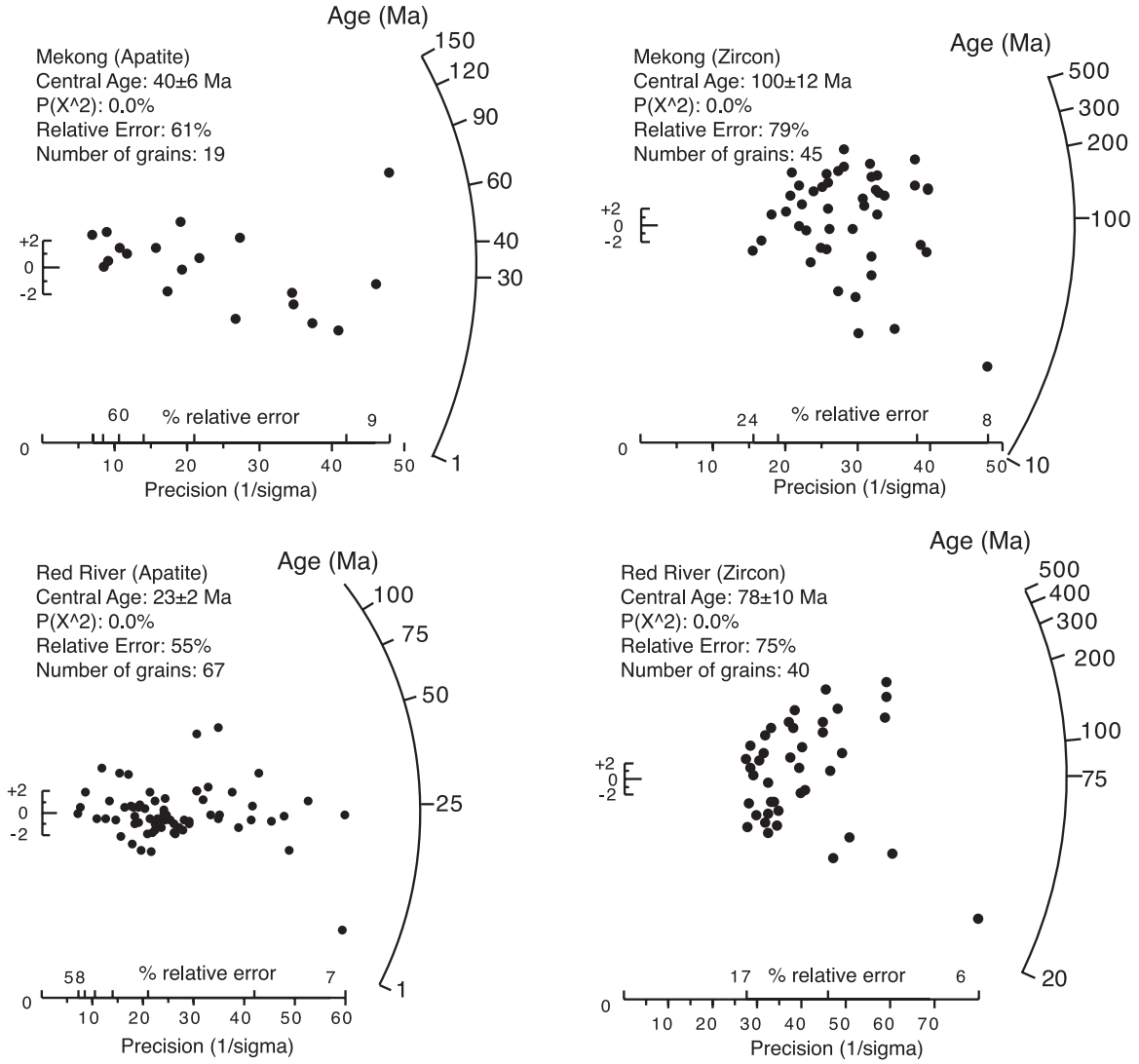

Figure 8. Radial plots of apatite and zircon fission track data for sediment samples taken from both the Mekong and Red Rivers. Plot shows the cooling ages of the individual grains in each sample combined with its uncertainty. Age is shown by the curved vertical axis, while the horizontal position shows the uncertainty [*Galbraith*, 1990]. Arrays of grains projecting to a point on the curved axis define populations with similar cooling histories.

ing both the age and the uncertainty of any given grain to be assessed [*Galbraith*, 1990]. Radial plots are designed to display single grain fission track data in preference to use of probability density diagrams. Probability plots are a type of continuous histogram that plots each grain age error as a Gaussian density function. All of the data are combined into a single continuous curve that has a shape comprising peaks and troughs according to the different age components and errors inherent to the component grain ages. Thus high precision age modes have narrow curves and less precise ages have broader curves. Ar-Ar mica and U-Pb ages generally have small errors with the result that probability plots provide an easy way of visibly comparing relative abundances of age modes (fingerprinting) between samples. However, there are several problems with this type of approach when applying it to fission track data or any data set with a large heterogeneous mix of uncertainties. The effect of plotting such data sets on a probability density diagram is to obscure useful information by inappropriately weighting curves with poor information, i.e., an overlap effect associated with broad, imprecise peaks, resulting in apparent age modes that do not necessarily correspond with the true age components. Radial plots in contrast do not have this presentational ambiguity.

[29] In the case of the zircon fission track analyses (ZFTA) the Red River appears to comprise two groups of source ages, one slightly older than

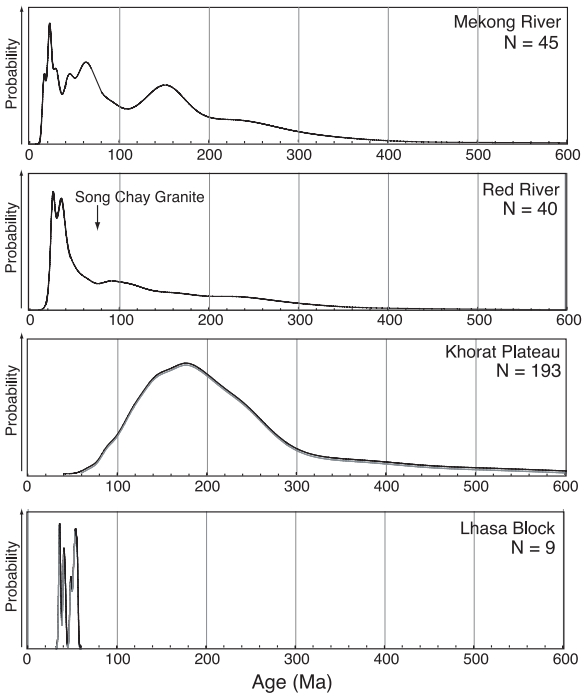

Figure 9. Probability density diagrams for zircon fission track ages from sands in the modern Mekong and Red Rivers compared with those known from possible source terrains in eastern Asia. Data from Khorat Plateau are from *Carter and Moss* [1999]. Data from the Lhasa Block are from *Yang et al.* [1999]. Point data on the Song Chay Granite are from *Roger et al.* [2000].

20 Ma and another around 200–400 Ma. The Mekong ZFTA are similar and although it also has a minority population of young grains (20–40 Ma), the majority of grain ages plot between 300 and 100 Ma. The lack of a well-defined population suggests either erosion from a slowly cooled terrain, or erosion from several terrains with different cooling histories. The apatite fission track analysis (AFTA) reveals a simpler exhumation history for both basins in showing a dominant range of 10–30 Ma for cooling through the apatite partial annealing zone (60–110°C; Figures 8 and 11). The differences between AFTA and ZFTA results indicate that even though the older, hotter parts of the exhumation histories of the dominant sources differ, the most important sources to both Red and Mekong Rivers have all seen rapid cooling during the interval 20–40 Ma.

7.1. Zircon Fission Track Results

[30] The potential provenance of the zircon grains can be seen in Figure 9 where probability density diagrams compare the ZFT ages of the river sands with those from the few sources for which matching bedrock data exist. As noted above this type of figure is not ideal for detailed analysis of fission track data and we use the superior radial plots (Figure 8) for determining age modes and to estimate relative abundances. However, their use is justified here for simple visual comparison purposes to show differences in the underlying age structure between river sediments and their potential sources. Comparison of radial plots between sources and sediment is more difficult to quickly digest and understand. Use of the ZFTA data is limited because the sample sizes are modest, comprising 40 and 45 grains. *Brandon* [2002] has argued that 100 grains are required in a mixed sedimentary source to derive a statistically robust result and identify the major grains populations. Similarly *Ruhl and Hodges* [2005] suggested that at least 50 grains are required to characterize erosion in a drainage with a relatively simple exhumation history, while more grains are required when sources are more numerous. The present study is thus limited to a first-order definition of the major sediment sources, but sample sizes are not big enough to robustly define or date all the minority sources contributing to either river. This is likely more problematic in the larger and more geologically complex Mekong drainage, compared to the simpler Red River basin.

[31] Unfortunately many of the sources regions have no bedrock data sets to match the detrital ages, which currently limits the use of this dating technique as a provenance tool. However, ZFTA results from the Khorat Plateau of central Indochina show that this cannot be a dominant source of sediment into the modern Mekong River, although modest erosion from this terrain could account for some of the tail of older ages seen in the Mekong sample (120–180 Ma; Figure 9) [*Carter and Bristow*, 2003]. ZFTA from the Lhasa Block [*Yang et al.*, 1999] shows that parts of Tibet were cooled by tectonic exhumation since 60 Ma and similar processes could have generated grains within the Qiangtang Block that are now present as sand in the Mekong. It is noteworthy that although exhumation within the Red River Fault Zone itself may be a possible source for the younger grains (<40 Ma) seen in the Red River sand, dating of granite in the nearby Song Chay Dome revealed ages too old to be significant to the total sediment budget [*Roger et al.*, 2000].

7.2. Apatite Fission Track Results

[32] Figure 10 shows the range of AFTA results from the river sands, together with those sources for which matching data exist. The relative sim-

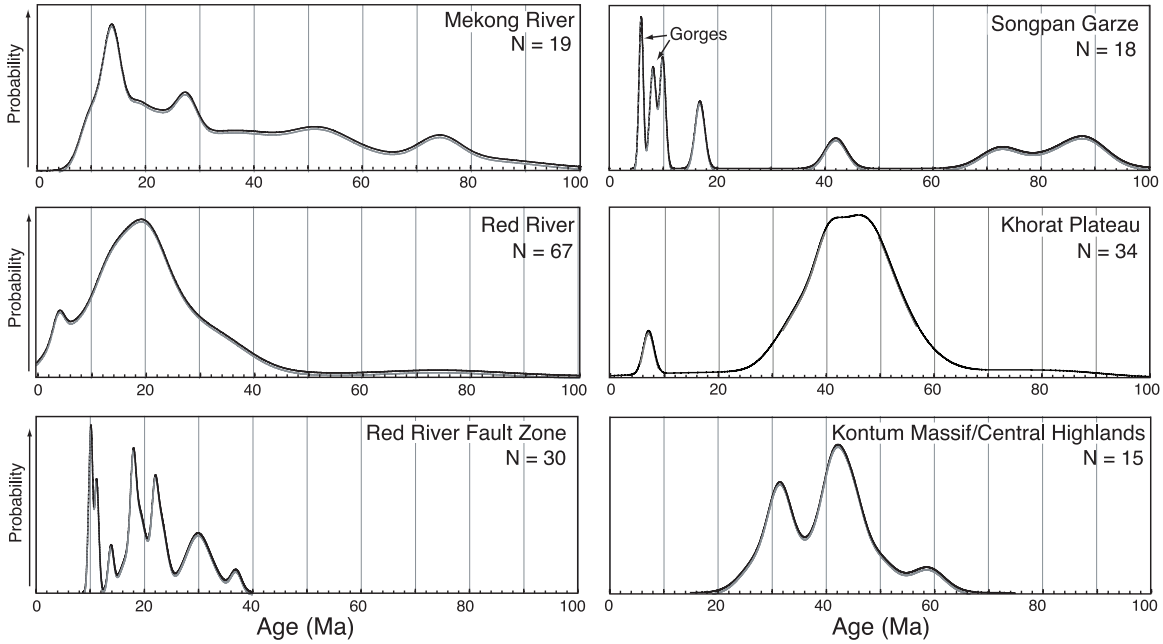

Figure 10. Probability density diagrams for apatite fission track ages from sands in the modern Mekong and Red Rivers compared with those from possible source terrains in eastern Asia. Data from the Ailao Shan/Red River Fault Zone are from *Bergman et al.* [1997] and *Maluski et al.* [2001]. Data from the Khorat Plateau are from *Racey et al.* [1997] and *Upton* [1999]. Data from the Songpan Garze Terrane are from *Reid et al.* [2005]. Data from the Kontum Massif are from *Carter et al.* [2000].

plicity of bedrock cooling in the modern Red River catchment and the number of grains considered (67) gives confidence that our analysis is yielding an accurate image of source exhumation. In contrast, only 19 grains were analyzed for AFTA from the Mekong, which also has a larger and more diverse source region. Consequently, conclusions concerning source exhumation from the Mekong sands must be considered to be of low reliability, at least when characterizing input from minority sources.

[33] The Red River sands show a remarkable good match with fission track ages measured in the Red River Fault Zone, which is a surprise given the U-Pb and Ar-Ar data that show the metamorphic rocks within the fault zones cannot be significant sources to the river. The AFTA data indicate that the Red River is being fed by sources that cooled from the apatite partial annealing zone (broadly 60–110°C for common apatite compositions [*Green et al.*, 1989]) since the Oligocene. Potentially this sediment is from rocks exposed adjacent to the metamorphic core of that shear zone, that did not suffer the deep exhumation of the gneisses, but which were uplifted and exhumed to a lesser extent during motion along that structure. Mesozoic and Cenozoic sedimentary basins close to the Red River Fault Zone in Yunnan, such as the Simao and Chuxiong Basins (Figure 3) were inverted during the period of left-lateral motion at 34–17 Ma [*Leloup et al.*, 1995; *Lacassin et al.*, 1997], and could be the sources of much of this material. With the exception of a few tectonically active zones, sources on the Tibetan Plateau itself cooled below the partial annealing zone too long ago to be major sediment sources. However, AFTA of rocks exposed in the gorges of Yunnan [*Clark et al.*, 2005] yielded apatite ages of 4–16 Ma that could be supplying young grains into the rivers from outside the immediate vicinity of the shear zones.

[34] We conclude that the ZFTA and AFTA of Mekong and Red River sands shows that erosion has been dominantly from rocks that cooled at the shallowest levels of the crust during the Cenozoic and that this is likely linked to either tectonic processes driven by large-scale strike-slip faulting (e.g., the Simao and Chuxiong Basins), and/or to gorge incision during regional uplift of eastern Tibet and Yunnan. Additional minor flux into the Mekong River has occurred from more slowly cooled terrains, such as the Khorat Plateau. Rapid exhumation of the Vietnamese Central Highlands since ~10 Ma may also have contributed material to that system [*Carter et al.*, 2000]. However, because the Central Highlands has a similar Trias-

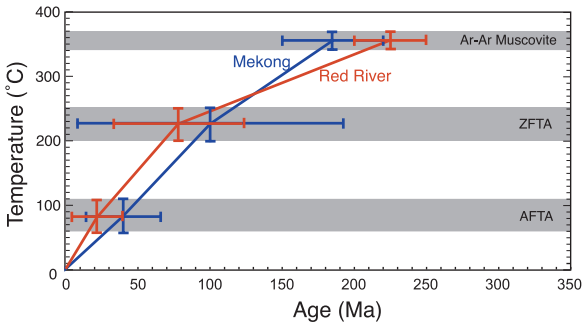

Figure 11. Hypothetic exhumation history of a typical sediment source to the Mekong and Red Rivers since the Triassic. Fission track central ages are plotted together with error bars showing the range of the partial annealing zones in apatite and zircon as well as the range of 95% of the dated grains.

sic Ar-Ar cooling age and Cenozoic exhumation history to the shear zones of eastern Tibet the relative influence of this terrain in feeding sediment to the Mekong is not resolvable with the methods used in this study.

8. Discussion

8.1. Source Exhumation

[35] The cooling history of sand grains now found close to the mouths of the Mekong and Red Rivers can be used to make general observations about the history of exhumation on a regional scale within the current drainage basins (Figure 11). The U-Pb ages measured from zircon grains constrain the timing of cooling below ~750°C, corresponding to igneous crystallization. Because there is a wide range of these ages in each basin we infer that the crust in each drainage was formed in a series of events spread over the last 2500 my, but this tells us little about when these rocks were exhumed. Instead the mica Ar-Ar and fission track methods can be used to get a regional picture of exhumation. Following the guidelines of *Brandon* [2002] and *Ruhl and Hodges* [2005] such estimates are much more accurate for the Red River where the number of apatite fission track analyses is higher (67) and the exhumation history is simpler than the larger, more tectonically diverse Mekong drainage. Zircon fission and Ar-Ar mica age analyses are just below but close to the 50 grain threshold of *Ruhl and Hodges* [2005] for the Red River, but can only provide a poorly constrained image of the Mekong.

[36] Ar-Ar mica ages in both basins fall approximately into two groups, a Cenozoic and the dominant Indosinian population, with a small number of 400–500 Ma grains found only in the Red River (Figure 6). These ages correspond to the time at which the sources cooled through the 350°C isotherm. Similarly the ZFTA can be used to date when these same rocks cooled through the 200–310°C partial annealing zone [*Tagami et al.*, 1998]. Although there is a spread, reflecting source diversity, most of the ZFT ages fall in the 20–140 Ma range in the Red River and from 10–200 Ma in the Mekong River (Figure 9).

[37] The shallowest cooling through the apatite partial annealing zone is constrained by the 0–40 Ma and 5–60 Ma AFT age ranges from the Red and Mekong Rivers respectively (Figure 10). The low number of AFT analyses for the Mekong makes it impossible image the diversity of shallow source exhumation histories in this basin because small, minority populations will not be covered in such a data set. Nonetheless, the FT data can provide limited control on the exhumation histories of the major sources, as has been shown by similar studies in the Indus River [*Clift et al.*, 2004b]. At a regional scale these data provide us with an image of how rapidly large areas of East Asia were exhumed over long periods of geologic time. Initial cooling from 350°C to ~200°C after the Indosinian Orogeny appears to have been slower on average in the Red compared to the Mekong basin. Indeed the presence of some Caledonian Ar-Ar ages tells us that some parts of the Red River basin experienced very slow Mesozoic exhumation. Cooling below the 200°C isotherm then appears to have been faster in the Red River basin, and this is well resolved for the shallowest exhumation from the apatite partial annealing zone to the modern surface (~2.4–4.4 km). AFT ages appears to be more skewed to younger values (<40 Ma) in the Red River basin compared to the Mekong, where there is a wider range of relatively older AFT ages (Figure 10). Average recent exhumation rates for the sources in the Red and Mekong River Basins are 104–191 m/Myr and 60–110 m/Myr respectively, assuming a 25°C/km thermal gradient.

[38] The low number of AFT analyses (19) from the Mekong sands means that only the shallow cooling rates of the most dominant sources are constrained, while minority sources cannot be resolved. Nonetheless, the first-order differences between the data sets make geological sense because the modern Red River basin is dominated by the relatively simple tectonic evolution of the Red River Fault Zone, whose activity from 17–34 Ma [*Maluski et al.*, 2001; *Gilley et al.*, 2003] is

responsible for much of the broad-scale exhumation patterns in that system. In contrast, the Mekong River covers a much wider area, spanning not only Cenozoic shear zones, but also Mesozoic Tibetan orogenic belts, and the Cretaceous Khorat sedimentary basin that was inverted during the Cenozoic [*Carter and Bristow*, 2003]. Not all these Mekong source areas have experienced rapid Cenozoic exhumation, but the number of analyses available here do not allow the detailed character of the source exhumation histories to be reconstructed.

[39] Limited regional AFT data from bedrock samples in Vietnam and Thailand [*Carter et al.*, 2000; *Maluski et al.*, 2001; *Upton*, 1999] show that since 20 Ma the depth of crust lost to erosion would not have exceeded 1500–2000 m, i.e., average regional erosion rates were ~75–100 m/Myr. Although the number of bedrock analyses is also not high the reconstructed rates of exhumation are much more robust than those derived from the sediments because samples from source terrains are not mixed and are thus much more readily modeled. Exhumation rates from the bedrock, together with those derived from the AFTA of the river sediments can be compared with denudation rate estimates calculated from the volumes of eroded sediment in the offshore region [*Clift et al.*, 2004a]. Using a 35% average porosity the volume of eroded rock is estimated at 46,000 km^3 and 24,300 km^3 for the Pleistocene in the Red and Mekong offshore basins respectively. These values in turn yield average Pleistocene denudation rates of around 178 m/Myr and 20 m/Myr in the Red and Mekong basins respectively (uncertainties are ±20% for the sedimentary budgets).

[40] The Red River basin exhumation rates calculated from sediment volumes and from the river sediment AFT data are within error of one another. However, in the Mekong there is an apparent discrepancy between the regional AFT data and offshore sediment accumulations. This difference may be linked to the small sample size, but could also reflect lithological diversity in that drainage. The youngest beds of the Khorat Basin of eastern Thailand and Laos through which the Mekong flows contained up to 1 km of evaporites. Erosion of these beds would have been imprinted on the regional bedrock AFT data but not recorded in the river sediments. Also the lower Mekong sediment yield rate probably reflects the fact that large areas of the Mekong basin are eroding slowly and may be even depositional in the floodplains of Indochina. In contrast, the Red River basin is largely mountainous, with a small coastal plain adjacent to the delta.

8.2. Provenance Synthesis

[41] The combination of the four dating methods employed here can be used to constrain the provenance of the sediment now found in the modern river mouths. Compared to some basins this is a relatively complicated task, because so much of Southeast Asia is affected by the Indosinian Orogeny and both basins show quite similar crustal generation histories in terms of their U-Pb zircon ages, resulting in small differences in the sources that can be transferred to the river sediments. Nonetheless, the U-Pb of the Red River sands do show a stronger affinity to Yangtze Craton sources than seen in the Mekong, specifically the abundance of both 700–800 Ma grains of Jinningian provenance and 1800–2000 Ma grains of Luliangian provenance that are rare in the Mekong (Figure 4). On closer analysis the Triassic Indosinian grains in the Mekong were seen to be younger than those in the Red River, a pattern that suggested an origin within the Tibetan Qiangtang Block or related units for Mekong sands. The origin of Indosinian grains in the Red River is less clear, but comparison with basement units favors erosion of blocks similar in their crustal genesis to the Kontum Massif or Khorat Plateau (Figure 4).

[42] Ar-Ar mica dates help constrain the provenance more closely. Again a strong flux from the Yangtze Craton into the Red River is suggested by a significant population of 350–500 Ma age grains in that river, matching an event best known in the southern Yangtze Craton (Figure 6) [*Chen and Jahn*, 1998]. The mica data show that the Indosinian ages in the Mekong and Red Rivers are resolvably different, as also seen for the U-Pb zircon ages. While the Red River Indosinian mica ages match sources forming part of Indochina, as well as the Qiangtang Block (the Ar-Ar history of the Yangtze Block is not known), the same cannot be said of the Mekong where the bias to younger values more closely matches erosion from the Qiangtang Block (Figure 6).

[43] Evidence from the fission track minerals at first seems contradictory to the logic derived from the U-Pb and Ar-Ar dating. The FTA of the Red River sands suggests a good match with the metamorphic rocks of the Red River Fault Zone (Figure 10), yet major erosion from the metamorphic rocks of that zone is precluded by the U-Pb

and to a lesser extent the Ar-Ar results. We infer that the sources now providing most of the sediment into the Red River experienced cooling through the uppermost 4–5 km of crust synchronous with motion along the Red River Fault Zone and its associated structures, yet these sources did not experience the deep exhumation associated with the high-grade rocks in the middle of the fault zone. The sediment in the Red River appears to have been generated due to a shallower and more regional exhumation process than that operating in the core of the fault zone. We infer that large volumes of sediment are being recycled from the Mesozoic and Cenozoic sequences in the Simao, Chuxiong and associated basins developed close to the fault zone (Figure 3). These were inverted during the phase of major left-lateral motion [*Leloup et al.*, 1995; *Lacassin et al.*, 1997] and would have Mesozoic high temperature ages, but Miocene AFT ages. In addition, sediment must be generated by gorge incision during uplift of eastern Tibet.

[44] Provenance in the Mekong basin is more complicated to explain and less well constrained than for the Red River because although there is a peak in the AFT ages in the last 25 Ma there is a significant tail of older values stretching back to 80 Ma. This tail likely reflects erosion from a number of slowly cooling minority sources. The low number of AFT ages from the Mekong prevents these from being resolved. Nonetheless, even at this first-order level differences between the Mekong and Red Rivers are apparent and make sense in the context of the regional geology. The Mekong is not so strongly associated with a major strike-slip fault zone as the Red River is, but the river does incise deep gorges in the eastern flanks of Tibet within Qiangtang Block crust, where the vertical incision reaches a maximum of 2500 m, sufficient to cool material from the apatite partial annealing zone. Although not located in the Mekong drainage, *Clark et al.* [2005] recorded AFT ages of 4–16 Ma in the Yangtze River gorges of Yunnan, and similar ages might be expected in the upper parts of the Mekong catchment, accounting for the peak in younger AFT ages. AFT ages around 30–50 Ma are consistent with known source regions in eastern Thailand and the Khorat Basin/Plateau (Figure 10) [*Upton*, 1999]. The older ages seen in ZFTA and FTA in the Mekong River may partially reflect erosion of the shallower parts of the gorges, where cooling must have been earlier than for rocks now exposed deep in the gorge. In addition, some material with older ages may be contributed from erosion within Indochina itself. FTA ages between 30 and 50 Ma are known from the Kontum Massif and Khorat Plateau (Figure 10) [*Carter et al.*, 2000; *Carter and Bristow*, 2003] and may have contributed sediment to the river, generating the long tail of older ages.

8.3. Controls on Erosion

[45] Having constrained the provenance of each of the rivers studied here using the thermochronology data presented above we are in position to assess what might be driving the erosion in the modern drainage. Competing potential controls include topography, modern tectonic rock uplift rates and climate, especially precipitation. Active tectonism can accentuate erosion rates through triggering land sliding by seismic shaking, as well as through rock uplift increasing the average gradient between source and sink [e.g., *Burbank et al.*, 2003; *Dadson et al.*, 2003]. Steeper slopes in turn cause gorge incision into bedrock. We test this hypothesis by comparing evidence for current tectonism and erosion patterns. Figure 12 shows the distribution of earthquakes above magnitude 5 recorded since 1964 in the eastern Tibet region. It is evident that the Red River Fault is now mostly inactive, as inferred from structural studies [*Leloup et al.*, 1993, 2001]. The cluster of earthquakes south of Kunming largely lies in the Pearl River drainage, meaning that active seismicity within the Red River drainage is mostly limited to a narrow strip of terrain within the Sibumasu Block, south of the Red River Fault Zone (Figures 2, 3, and 12). This pattern of activity bears little resemblance to the erosion, which is focused on those regions recently exhumed in the broad vicinity of the Red River Fault Zone, and with a significant contribution from the Yangtze Craton, lying north of the modern river. Seismicity in the Mekong basin is strong around 22–24°N and 100–101°E, involving units of the Sibumasu Block and the Changning-Menglian Block. These units may be important contributors to the river but do not dominate the bedload, which is drawn partially from units in southern and central Indochina, but mostly from the incised gorges in the edge of the Qiangtang Block.

[46] The relationship between solid Earth tectonic motions and erosion can also be assessed by looking at modern rates of motion recorded by GPS surveying [e.g., *Shen et al.*, 2000; *Chen et al.*, 2000; *England and Molnar*, 2005; *Meade*, 2006]. Unfortunately vertical motions are hard to resolve

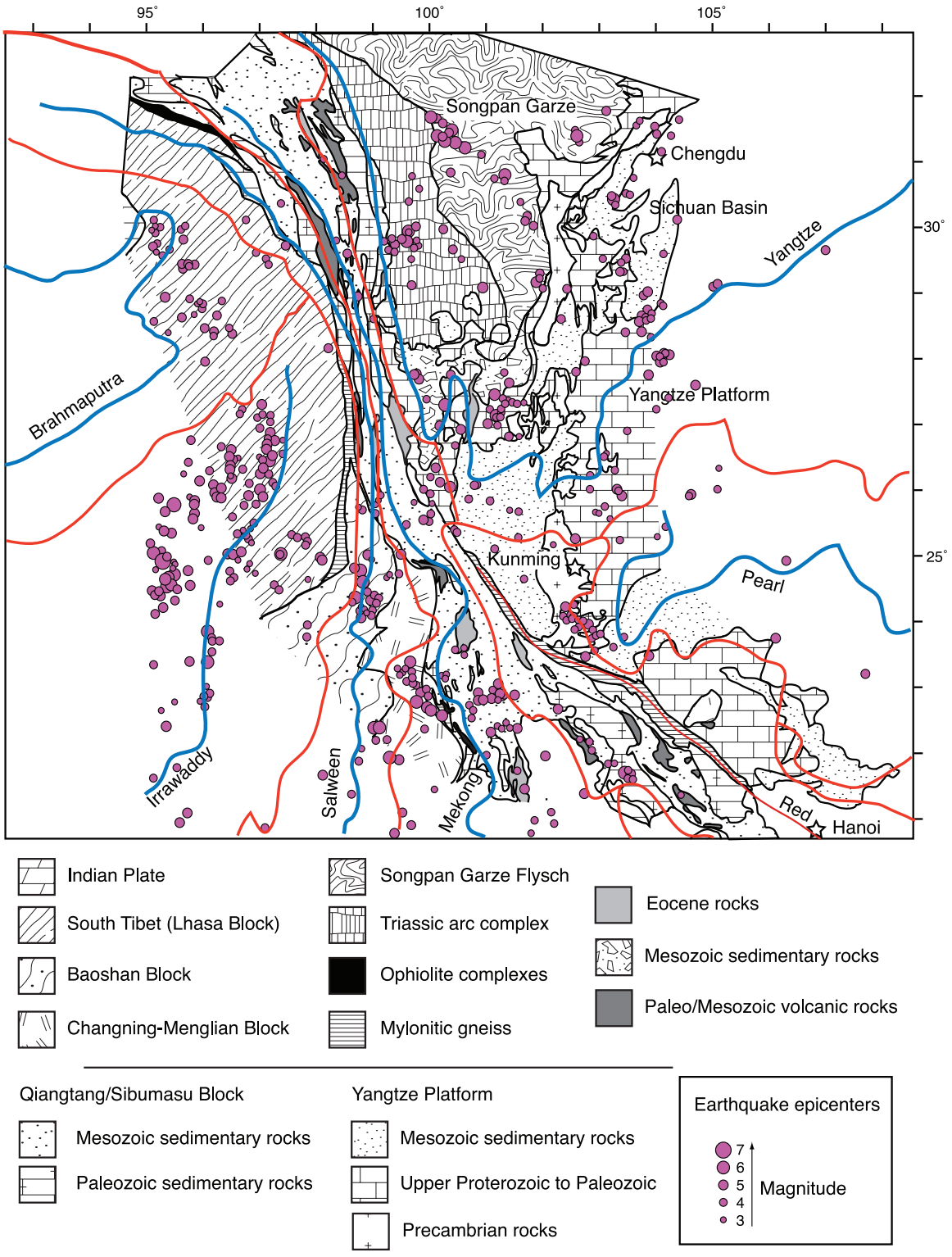

Figure 12. Map showing the geology of eastern Tibetan Plateau, SW China, and northern Indochina overlain by the epicenters of earthquakes above magnitude 3 recorded since 1965 shown as pink dots. Smallest diameter dots represent the smallest magnitude events, ranging down to magnitude 3. Earthquake data are from the compilation of GeoMapApp. Rivers are shown as blue lines, with the edge of their drainage basins shown in red.

with this methodology, yet the horizontal motion of crustal blocks does provide an image of how the crust is being strained and may provide some indication of how erosion might be linked to this process. Motions recorded by GPS parallel the viscous flow of lower crust, extruded eastward from Tibet [e.g., *Clark and Royden*, 2000]. Figure 13 shows the deformation field modeled by *Meade* [2006] based on the GPS data of *Chen et al.* [2000], in which the motion is plotted relative to stable Eurasia, overlain on the regional geological map. Tectonic motions are dominantly toward the southeast and are most rapid in eastern Tibet, where we infer strong erosion in the gorges cutting the Qiangtang Block. Rapid motions are observed in the northeastern part of the Red River drainage, consistent with erosion of deformed Yangtze Craton units into that system. Active displacement also affects the northern areas surrounding the Red River Fault Zone, including the Simao and Chuxiong Basins that form the likely dominant source of material to the river. We conclude that there is a relatively good correlation between rates of tectonic deformation and erosion, but no strong link with seismicity.

[47] Finally we compare erosion with precipitation patterns across the region (Figure 14) in an attempt to test hypotheses that it is rainfall that is the dominant control on erosion [e.g., *Galy and France-Lanord*, 2001; *Reiners et al.*, 2003; *Wobus et al.*, 2003; *Thiede et al.*, 2004; *Bookhagen et al.*, 2005; *Clift*, 2006]. Rainfall is heavy throughout the Red River basin, although less so in the north close to Kunming. In the Mekong basin rainfall is low in its headwaters on the Tibetan Plateau, but is higher moving south into the gorges around 28–25°N latitude. Precipitation is heavier still at 22–24°N in the same region of heaviest seismic activity. Although not plotted on Figure 14 precipitation is very heavy in Indochina in the Kontum Massif and Central Highlands of Vietnam, which we infer to be only moderate contributors to the river. The strongest sediment-generating region of the Mekong basin in the gorges of eastern Tibet is not the region of heaviest rainfall.

[48] We conclude that the steep margins of the Tibetan Plateau in regions of active tectonic strain are the most important sediment producers in each river system. While an absence of rain inhibits erosion on the Tibetan Plateau and rain is an important process in driving erosion in Indochina, it is most efficient as an erosive agent only when accompanied by active rock uplift [*Whipple et al.*, 1999].

9. Conclusions

[49] In this study we have shown that a combination of U-Pb dating of zircon grains, $^{40}Ar/^{39}Ar$ dating of micas and fission track analysis of apatite and zircon grains can be employed to constrain the provenance of sediment in the modern Red and Mekong Rivers, and furthermore provides us with an image of how the crust in Southeast Asia was first built, then deformed and uplifted over long periods of geologic time. As noted by *Campbell et al.* [2005] and *Carter and Bristow* [2000] U-Pb dating of zircon alone can provide a misleading picture of provenance because of multiple reworking of these mineral grains through sedimentary systems. Fortunately we have additional evidence from other mineral groups to support provenance conclusions in this study. In the case of the Red and Mekong Rivers we see that although the crust was constructed in a series of Paleozoic and Precambrian stages it was largely reset with regard to the $^{40}Ar/^{39}Ar$ system during the Triassic, albeit with noteworthy diachroneity between older deformation in the Red and younger in the Mekong basins. Both $^{40}Ar/^{39}Ar$ and U-Pb evidence indicates greater erosional flux from Yangtze Cratonic sources into the Red River compared to the Mekong.

[50] Apatite and zircon fission track analyses record a range of cooling ages that include evidence for accelerated cooling in the sources of the Red River since 25 Ma. Most of these source ages are related to exhumation within the Red River basin during activity of the Red River Fault Zone, although inverted and incised sedimentary basins, such as the Simao and Chuxiong Basins (Figure 3) are likely the most important sources of sediment to the modern river. U-Pb and $^{40}Ar/^{39}Ar$ data demonstrate that the high-grade metamorphic rocks that form the core of the Red River Fault Zone only provide a small percentage of the total sediment flux. Sparse AFT data suggest that most sediment in the Mekong River comes from sources that have cooled from 60–110°C since 40 Ma, but that slower cooling terrains also seem to be contributing. However, small sample size precludes unique identification and dating of these sources at this time. Data from all thermochronologic methods suggests that gorge incision into the crust of the Tibetan Qiangtang Block and its equivalent units in Indochina (Sibumasu Block) is the dominant source of sediment into the Mekong River.

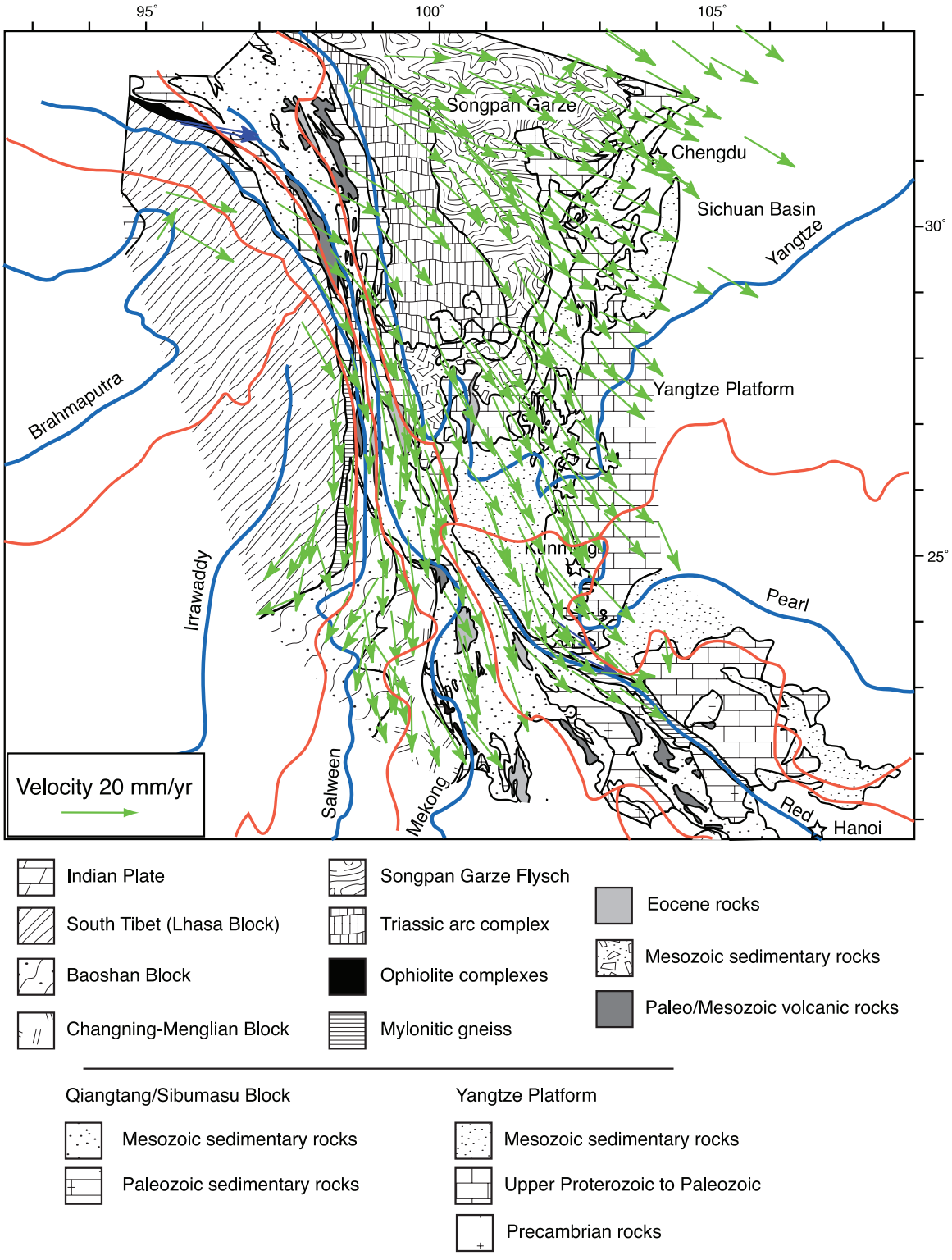

Figure 13. Map showing the geology of eastern Tibetan Plateau, SW China, and northern Indochina overlain by arrows showing the present-day rates of horizontal crustal motion relative to a stable Eurasia continent, measured by GPS [*Chen et al.*, 2000] and modeled by *Meade* [2006]. Rivers are shown as blue lines, with the edge of their drainage basins shown in red.

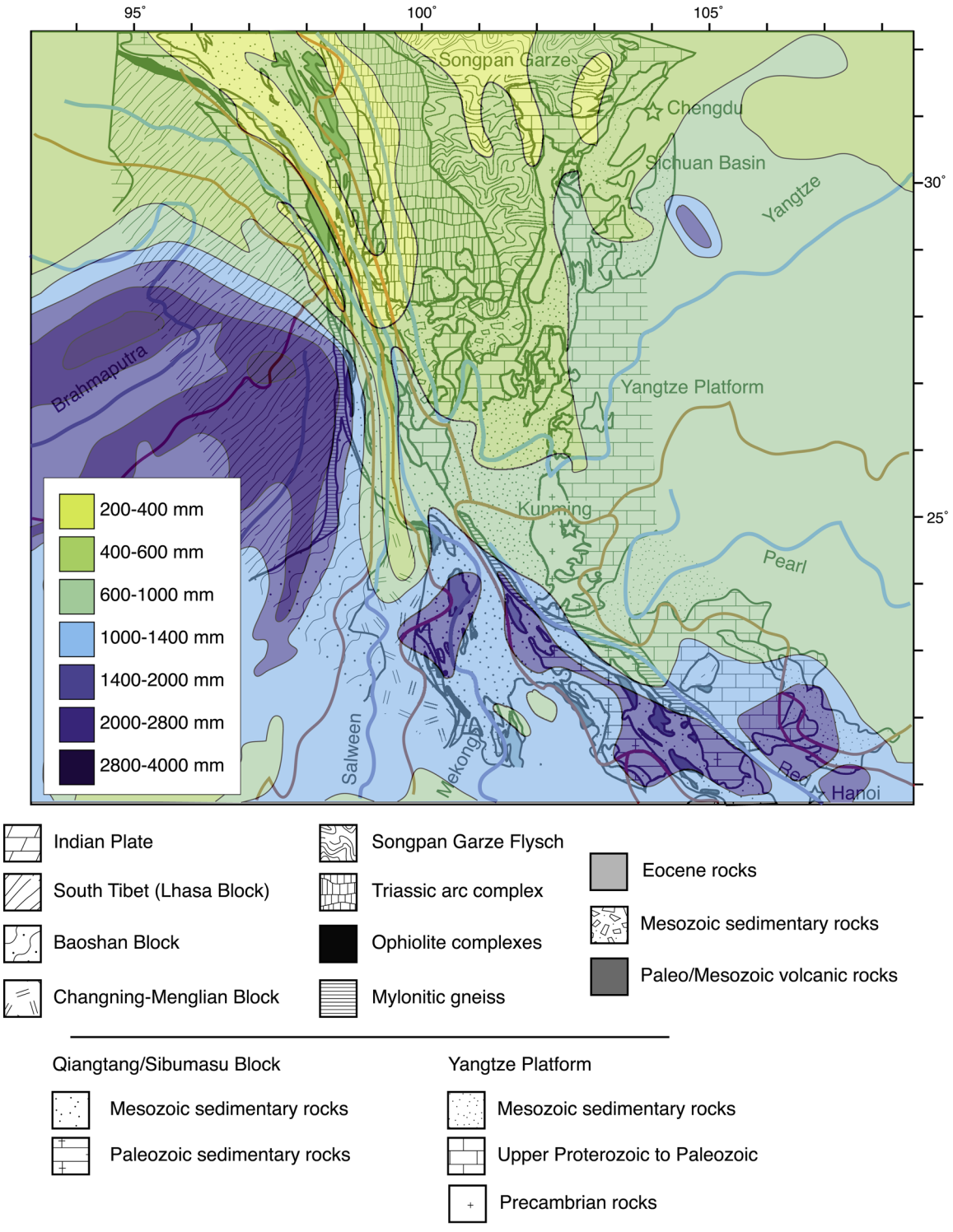

Figure 14. Map showing the geology of eastern Tibetan Plateau, SW China, and northern Indochina overlain by annual precipitation amounts taken from National Geographic Society database. Rivers are shown as blue lines, with the edge of their drainage basins shown in red.

[51] Much of the erosion in both rivers is caused by gorge incision driven by active rock uplift of the Tibetan Plateau in the presence of significant precipitation. Heavier precipitation in southern Indochina does not result in similar rapid erosion, underlying the importance of rock uplift driven by plate tectonic forces as being the primary control on erosion. Rainfall is nonetheless an important

secondary control because it can drive moderate erosion where tectonism is inactive, such as in southern Indochina, and prevents erosion in tectonically active regions such as the Tibetan Plateau, where there is little precipitation.

Acknowledgments

[52] P.C. wishes to thank Brad Hacker, Alfred Kroener, Lothar Ratschbacher, Francois Roger, Urs Schärer, and Stuart Gilder for their help in collating radiometric age and isotopic data from many sources as part of this study. Marin Clark, Barbara Carrapa, and editor Vincent Salters are thanked for their helpful, critical reviews. Lars Henrik Nielsen helped in the collection of the samples. Brendan Meade is thanked for his help with GPS data. The costs of this study were partially covered by the University of Aberdeen. We thank B. C. Burchfiel and C. Studnicki-Gizbert for their help with geological maps and on advice with GPS data sources.

References

Bergman, S. C., P. H. Leloup, P. Tapponnier, U. Schärer, and P. O'Sullivan (1997), Apatite fission track thermal history of the Ailao Shan-Red River shear zone, China, paper presented at European Union of Geosciences, Strasbourg, France, 23–27 March.

Black, L. P., et al. (2004), Improved $^{206}Pb/^{238}U$ microprobe geochronology by the monitoring of a trace-element-related matrix effect; SHRIMP, ID-TIMS, ELA-ICP-MS and oxygen isotope documentation for a series of zircon standards, *Chem. Geol.*, *205*, 115–140.

Bodet, F., and U. Schärer (2001), Pb isotope systematics and time-integrated Th/U of SE-Asian continental crust recorded by single K-feldspar grains in large rivers, *Chem. Geol.*, *177*, 265–285.

Bookhagen, B., R. C. Thiede, and M. R. Strecker (2005), Abnormal monsoon years and their control on erosion and sediment flux in the high, arid northwest Himalaya, *Earth Planet. Sci. Lett.*, *231*, 131–146.

Brandon, M. T. (2002), Decomposition of mixed age distributions using BINOMFIT, *On Track*, *24*, 13–18.

Brookfield, M. E. (1998), The evolution of the great river systems of southern Asia during the Cenozoic India-Asia collision: Rivers draining southwards, *Geomorphology*, *22*, 285–312.

Bruguier, O., J. R. Lancelot, and J. Malavieille (1997), U-Pb dating on single detrital zircon grains from the Triassic Songpan-Ganze Flysch (central China): Provenance and tectonic correlations, *Earth Planet. Sci. Lett.*, *152*, 217–231.

Burbank, D. W., A. E. Blythe, J. Putkonen, B. Pratt-Sitaula, E. Gabet, M. Oskins, A. Barros, and T. P. Ojha (2003), Decoupling of erosion and precipitation in the Himalayas, *Nature*, *426*, 652–655.

Campbell, I. H., P. W. Reiners, C. M. Allen, S. Nicolescu, and R. Upadhyay (2005), He-Pb double dating of detrital zircons from the Ganges and Indus Rivers: Implication for quantifying sediment recycling and provenance studies, *Earth Planet. Sci. Lett.*, *237*, 402–432.

Carter, A. (1999), Present status and future avenues of source region discrimination and characterisation using fission-track analysis, *Sediment. Geol.*, *124*, 31–45.

Carter, A., and C. S. Bristow (2000), Detrital zircon geochronology: Enhancing the quality of sedimentary source information through improved methodology and combined U-Pb and fission track techniques, *Basin Res.*, *12*, 47–57.

Carter, A., and C. S. Bristow (2003), Linking hinterland evolution and continental basin sedimentation by using detrital zircon thermochronology: A study of the Khorat Plateau basin, eastern Thailand, *Basin Res.*, *15*, 271–285.

Carter, A., and S. J. Moss (1999), Combined detrital-zircon fission-track and U-Pb dating: A new approach to understanding hinterland evolution, *Geology*, *27*, 235–238.

Carter, A., D. Roques, and C. S. Bristow (2000), Denudation history of onshore central Vietnam: Constraints on the Cenozoic evolution of the western margin of the South China Sea, *Tectonophysics*, *322*, 265–277.

Carter, A., D. Roques, C. Bristow, and P. Kinny (2001), Understanding Mesozoic accretion in Southeast Asia: Significance of Triassic thermotectonism (Indosinian orogeny) in Vietnam, *Geology*, *29*, 211–214.

Chen, J. F., and B. M. Jahn (1998), Crustal evolution of southeastern China: Nd and Sr isotopic evidence, *Tectonophysics*, *284*, 101–133.

Chen, J. F., J. Yan, Z. Xie, X. Xu, and F. Xing (2001), Nd and Sr isotopic compositions of igneous rocks from the Lower Yangtze region in Eastern China: Constraints and sources, *Phys. Chem. Earth, Part A*, *26*, 719–731.

Chen, Z., B. C. Burchfiel, Y. Liu, R. W. King, L. H. Royden, W. Tang, E. Wang, J. Zhao, and X. Zhang (2000), Global Positioning System measurements from eastern Tibet and their implications for India/Eurasia intercontinental deformation, *J. Geophys. Res.*, *105*, 16,215–16,227.

Cherniak, D. J., and E. B. Watson (2001), Pb diffusion in zircon, *Chem. Geol.*, *172*, 5–24.

China Geological Survey (2004), Geological Map of China (in Chinese), 1:2,500,000, China Geol. Map Press, Beijing.

Clark, M. K., and L. H. Royden (2000), Topographic ooze: Building the eastern margin of Tibet by lower crustal flow, *Geology*, *28*, 703–706.

Clark, M. K., L. M. Schoenbohm, L. H. Royden, K. X. Whipple, B. C. Burchfiel, X. Zhang, W. Tang, E. Wang, and L. Chen (2004), Surface uplift, tectonics, and erosion of eastern Tibet from large-scale drainage patterns, *Tectonics*, *23*, TC1006, doi:10.1029/2002TC001402.

Clark, M. K., M. A. House, L. H. Royden, K. X. Whipple, B. C. Burchfiel, X. Zhang, and W. Tang (2005), Late Cenozoic uplift of southeastern Tibet, *Geology*, *33*, 525–528.

Clift, P. D. (2006), Controls on the erosion of Cenozoic Asia and the flux of clastic sediment to the ocean, *Earth Planet. Sci. Lett.*, *241*, 571–580.

Clift, P. D., G. D. Layne, and J. Blusztajn (2004a), The erosional record of Tibetan uplift in the East Asian marginal seas, in *Continent-Ocean Interactions in the East Asian Marginal Seas*, edited by P. D. Clift, P. Wang, D. E. Hayes, and W. Kuhnt, *Am. Geophys. U., Geophys. Monogr*, 149, 255–282.

Clift, P. D., I. H. Campbell, M. S. Pringle, A. Carter, X. Zhang, K. V. Hodges, A. A. Khan, and C. M. Allen (2004b), Thermochronology of the modern Indus River bedload: New insight into the controls on the marine stratigraphic record, *Tectonics*, *23*, No. 5, TC5013, doi:10.1029/2003TC001559.

Clift, P. D., J. Blusztajn, and D. A. Nguyen (2006), Large-scale drainage capture and surface uplift in Eastern Tibet before 24 Ma, *Geophys. Res. Lett.*, doi:10.1029/2006GL027772, in press.

Corrigan, J. D., and K. D. Crowley (1990), Fission track analysis of detrital apatites from Sites 717 and 718, leg 116,

central Indian Ocean, *Proc. Ocean Drill. Program Sci. Results*, *116*, 75–92.

Dadson, S., et al. (2003), Links between erosion, runoff variability and seismicity in the Taiwan orogen, *Nature*, *426*, 648–651.

DeCelles, P. G., G. E. Gehrels, Y. Najman, A. J. Martin, A. Carter, and E. Garzanti (2004), Detrital geochronology and geochemistry of Cretaceous-early Miocene strata of Nepal: Implications for timing and diachroneity of initial Himalayan orogenesis, *Earth Planet. Sci. Lett.*, *227*, 313–330.

England, P., and P. Molnar (2005), Late Quaternary to decadal velocity fields in Asia, *J. Geophys. Res.*, *110*, B12401, doi:10.1029/2004JB003541.

Flower, M., K. Tamaki, and N. Hoang (1998), Mantle extrusion: A model for dispersed volcanism and DUPAL-like asthenosphere in East Asia and the western Pacific, in *Mantle Dynamics and Plate Interactions in East Asia*, *Geodyn. Ser.*, vol. 27, edited by M. F. J. Flower et al., pp. 67–88, AGU, Washington, D. C.

Galbraith, R. F. (1990), The radial plot: Graphical assessment of spread in ages, *Nucl. Tracks*, *17*, 207–214.

Galbraith, R. F., and P. F. Green (1990), Estimating the component ages in a finite mixture, *Nucl. Tracks Radiat. Meas.*, *17*, 197–206.

Galy, A., and C. France-Lanord (2001), Higher erosion rates in the Himalaya: Geochemical constraints on riverine fluxes, *Geology*, *29*, 23–26.

Gilder, S. A., J. B. Gill, R. S. Coe, X. Zhao, Z. Liu, G. Wang, K. Yuan, W. Liu, G. Kuang, and H. Wu (1996), Isotopic and paleomagnetic constraints on the Mesozoic tectonic evolution of South China, *J. Geophys. Res.*, *101*, 16,137–16,155.

Gilley, L. D., T. M. Harrison, P. H. Leloup, F. J. Ryerson, O. M. Lovera, and J. Wang (2003), Direct dating of left-lateral deformation along the Red River shear zone, China and Vietnam, *J. Geophys. Res.*, *108*(B2), 2127, doi:10.1029/2001JB001726.

Green, P. F., I. R. Duddy, G. M. Laslett, K. A. Hegarty, A. J. W. Gleadow, and J. F. Lovering (1989), Thermal annealing of fission tracks in apatite: 4 quantitative modeling techniques and extension to geological timescales, *Chem. Geol.*, *79*, 155–182.

Grimmer, J. C., R. Jonckheere, E. Enkelmann, L. Ratschbacher, B. R. Hacker, A. E. Blythe, G. A. Wagner, Q. Wu, S. Liu, and S. Dong (2002), Cretaceous-Cenozoic history of the southern Tan-Lu fault zone: Apatite fission-track and structural constraints from the Dabie Shan (eastern China), *Tectonophysics*, *359*, 225–253.

Grimmer, J. C., L. Ratschbacher, M. McWilliams, F. Leander, I. Gaitzsch, M. Tichomirowa, B. R. Hacker, and Y. Zhang (2003), When did the ultrahigh-pressure rocks reach the surface? A $^{207}Pb/^{206}Pb$ zircon, $^{40}Ar/^{39}Ar$ white mica, Si-in-white mica, single-grain provenance study of Dabie Shan synorogenic foreland sediments, *Chem. Geol.*, *197*, 87–110.

Hacker, B. R., L. Ratschbacher, L. Webb, T. R. Ireland, D. Walker, and S. Dong (1998), U/Pb zircon ages constrain the architecture of the ultrahigh-pressure Qinling-Dabie Orogen, China, *Earth Planet. Sci. Lett.*, *161*, 215–230.

Hacker, B. R., L. Ratschbacher, L. Webb, M. O. McWilliams, T. Ireland, A. Calvert, S. Dong, H. R. Wenk, and D. Chateigner (2000), Exhumation of ultrahigh-pressure continental crust in east central China: Late Triassic-Early Jurassic tectonic unroofing, *J. Geophys. Res.*, *105*, 13,339–13,364.

Hall, R. (2002), Cenozoic geological and plate tectonic evolution of SE Asia and the SW Pacific: Computer-based reconstructions, model and animations, *J. Asian Earth Sci.*, *20*, 353–434.

Harrison, T. M., P. H. Leloup, F. J. Ryerson, P. Tapponnier, R. Lacassin, and W. Chen (1996), Diachronous initiation of transtension along the Ailao Shan-Red River Shear Zone, Yunnan and Vietnam, in *The Tectonic Evolution of Asia*, edited by A. Yin and T. M. Harrison, pp. 208–226, Cambridge Univ. Press, New York.

Hodges, K. V. (2003), Geochronology and thermochronology in orogenic systems, in *Treatise on Geochemistry: The Crust*, edited by R. L. Rudnick, pp. 263–292, Elsevier, New York.

Huang, M., R. Maas, I. S. Buick, and I. S. Williams (2003), Crustal response to continental collisions between the Tibet, Indian, South China and North China blocks: Geochronological constraints from the Songpan-Garze orogenic belt, western China, *J. Metamorph. Geol.*, *21*, 223–240.

Hurford, A. J. (1990), Standardization of fission track dating calibration: Recommendation by the Fission Track Working Group of the I. U. G. S. subcommission on geochronology, *Chem. Geol.*, *80*, 177–178.

Jahn, B., P. Y. Chen, and T. P. Yen (1976), Rb-Sr ages of granitic rocks from southeastern China and their tectonic significance, *Bull. Geol. Soc. Am.*, *87*, 763–776.

Jolivet, L., H. Maluski, O. Beyssac, B. Goffe, C. Lepvrier, T. T. Phan, and V. V. Nguyen (1999), Oligocene-Miocene Bu Khang extensional gneiss dome in Vietnam: Geodynamic implications, *Geology*, *27*, 67–70.

Kapp, P., A. Yin, C. E. Manning, M. Murphy, T. M. Harrison, M. Spurlin, D. Lin, X. G. Deng, and C. M. Wu (2000), Blueschist-bearing metamorphic core complexes in the Qiangtang block reveal deep crustal structure of northern Tibet, *Geology*, *28*, 19–22.

Kapp, P., A. Yin, C. E. Manning, T. M. Harrison, M. H. Taylor, and L. Ding (2003), Tectonic evolution of the early Mesozoic blueschist-bearing Qiangtang metamorphic belt, central Tibet, *Tectonics*, *22*(4), 1043, doi:10.1029/2002TC001383.

Koppers, A. A. P. (2002), ArArCalc—Software for $^{40}Ar/^{39}Ar$ age calculation, *Comput. Geosci.*, *28*, 605–619.

Kroener, A., G. W. Zhang, and Y. Sun (1993), Granulites in the Tongbai area, Qinling Belt, China: Geochemistry, petrology, single zircon geochronology, and implications for the tectonic evolution of eastern Asia, *Tectonics*, *12*, 245–256.

Lacassin, R., H. Maluski, P. H. Leloup, P. Tapponnier, C. Hinthing, K. Siribhakdi, S. Chuaviroj, and A. Charoenravat (1997), Tertiary diachronic extrusion and deformation of western Indochina: Structural and $^{40}Ar/^{39}Ar$ evidence from NW Thailand, *J. Geophys. Res.*, *102*, 10,013–10,037.

Leloup, P. H., T. M. Harrison, F. J. Ryerson, W. Chen, Q. Li, P. Tapponnier, and R. Lacassin (1993), Structural, petrological and thermal evolution of a Tertiary ductile strike-slip shear zone, Diancang Shan, Yunnan, *J. Geophys. Res.*, *98*, 6715–6743.

Leloup, P. H., R. Lacassin, P. Tapponnier, U. Schärer, D. Zhong, X. Liu, L. Zhang, S. Ji, and T. T. Phan (1995), The Ailao Shan-Red River shear zone (Yunnan, China), Tertiary transform boundary of Indochina, *Tectonophysics*, *251*, 3–10.

Leloup, P. H., N. Arnaud, R. Lacassin, J. R. Kienast, T. M. Harrison, P. Trinh, A. Replumaz, and P. Tapponnier (2001), New constraints on the structure, thermochronology, and timing of the Ailao Shan-Red River shear zone, SE Asia, *J. Geophys. Res.*, *106*, 6683–6732.

Lepvrier, C., H. Maluski, V. V. Nguyen, D. Roques, V. Axente, and C. Rangin (1997), Indosinian NW-trending shear zones within the Truong Son Belt (Vietnam): ^{40}Ar-^{39}Ar Triassic

ages and Cretaceous to Cenozoic overprints, *Tectonophysics*, *283*, 105–127.

Li, W. X., X. H. Li, and Z. X. Li (2005), Neoproterozoic bimodal magmatism in the Cathaysia Block of South China and its tectonic significance, *Precambrian Res.*, *136*, 51–66.

Li, X., M. Tatsumoto, W. R. Premo, and X. Gui (1989), Age and origin of the Tanghu Granite, southeastern China: Results from U-Pb single zircon and Nd isotopes, *Geology*, *17*, 395–399.

Li, X. H. (1999), U-Pb zircon ages of granites from the southern margin of the Yangtze Block: Timing of Neoproterozoic Jinning orogeny in SE China and implications for Rodinia assembly, *Precambrian Res.*, *97*, 43–57.

Li, X. H., H. Zhou, S. L. Chung, S. Ding, Y. Liu, C. Y. Lee, W. Ge, and R. Zhang (2002), Geochemical and Sm-Nd isotopic characteristics of metabasites from central Hainan Island, South China and their tectonic significance, *Island Arc*, *11*, 193–205.

Li, Z. X., X. H. Li, H. Zhou, and P. D. Kinny (2001), Grenvillian continental collision in south China: New SHRIMP U-Pb zircon results and implications for the configuration of Rodinia, *Geology*, *30*, 163–166.

Ling, W., S. Gao, B. Zhang, H. Li, Y. Liu, and J. Cheng (2003), Neoproterozoic tectonic evolution of the northwestern Yangtze Craton, South China: Implications for amalgamation and break-up of the Rodinia supercontinent, *Precambrian Res.*, *122*, 111–140.

Lo, C., T. Lee, C. Lan, P. Wang, and T. V. Long (1999), Thermochronological study of the Kontum massif, central Vietnam and its implication to tectonothermal events in Indochina, *Eos Trans. AGU*, *80*(46), Fall Meet. Suppl., F1044.

Ma, C., C. Ehlers, C. Xu, Z. Li, and K. Yang (2000), The roots of the Dabieshan ultrahigh-pressure metamorphic terrane: Constraints from geochemistry and Nd-Sr isotope systematics, *Precambrian Res.*, *102*, 279–301.

Maluski, H., C. Lepvrier, L. Jolivet, A. Carter, D. Roques, O. Beyssac, T. T. Tang, D. T. Nguyen, and D. Avigad (2001), Ar-Ar and fission-track ages in the Song Chay Massif: Early Triassic and Cenozoic tectonics in northern Vietnam, *J. Asian Earth Sci.*, *19*, 233–248.

Meade, B. J. (2006), Present-day deformation at the India-Asia collision zone, *Geology*, in press.

Metcalfe, I. (1996), Pre-Cretaceous evolution of SE Asian terranes, in *Tectonic Evolution of SE Asia*, edited by R. Hall and D. J. Blundell, *Geol. Soc. Spec. Publ.*, *106*, 97–122.

Morley, C. K. (2002), A tectonic model for the Tertiary evolution of strike-slip faults and rift basins in SE Asia, *Tectonophysics*, *347*, 189–215.

Nagy, E. A., U. Schärer, and T. M. Nguyen (2000), Oligo-Miocene granitic magmatism in central Vietnam and implications for continental deformation in Indochina, *Terra Nova*, *12*, 67–76.

Nagy, E. A., H. Maluski, C. Lepvrier, U. Schärer, T. T. Phan, A. Leyreloup, and V. T. Vu (2001), Geodynamic significance of the Kontum Massif in central Vietnam: Composite $^{40}Ar/^{39}Ar$ and U-Pb ages from Paleozoic to Triassic, *J. Geol.*, *109*, 755–770.

Najman, Y., M. Pringle, L. Godin, and G. Oliver (2002), A reinterpretation of the Balakot Formation: Implications for the tectonics of the NW Himalaya, Pakistan, *Tectonics*, *21*(5), 1045, doi:10.1029/2001TC001337.

Pearce, N. J. G., W. T. Perkins, J. A. Westgate, M. P. Gorton, S. E. Jackson, C. R. Neal, and S. P. Chenery (1997), A compilation of new and published major and trace element data for NIST SRM 610 and NIST SRM 612 glass reference materials, *Geostand. Newsl.*, *21*, 115–144.

Racey, A., M. A. Love, A. C. Canham, J. G. S. Goodall, S. Polachan, and P. Jones (1996), Stratigraphy and reservoir potential of the Mesozoic Khorat Group, NE Thailand: Part 1, Stratigraphy and sedimentary evolution, *J. Pet. Geol.*, *19*, 5–39.

Racey, A., L. R. Duddy, and M. A. Love (1997), Apatite fission track analysis of Mesozoic red beds from northeastern Thailand and western Laos, in *Proceedings of the International Conference on Stratigraphy and Tectonic Evolution of Southeast Asia and the South Pacific*, edited by P. Dheeradilok et al., pp. 200–209, IGCP Research Program, Bangkok.

Reid, A. J., C. J. L. Wilson, and S. Liu (2005), Structural evidence for the Permo-Triassic tectonic evolution of the Yidun Arc, eastern Tibetan Plateau, *J. Struct. Geol.*, *27*, 119–137.

Reiners, P. W., T. A. Ehlers, S. G. Mitchell, and D. R. Montgomery (2003), Coupled spatial variations in precipitation and long-term erosion rates across the Washington Cascades, *Nature*, *426*, 645–647.

Renne, P. R., C. C. Swisher, A. L. Deino, D. B. Karner, T. Owens, and D. J. DePaolo (1998), Intercalibration of standards, absolute ages and uncertainties in $^{40}Ar/^{39}Ar$ dating, *Chem. Geol.*, *145*, 117–152.

Replumaz, A., and P. Tapponnier (2003), Reconstruction of the deformed collision zone Between India and Asia by backward motion of lithospheric blocks, *J. Geophys. Res.*, *108*(B6), 2285, doi:10.1029/2001JB000661.

Roger, F., P. H. Leloup, M. Jolivet, R. Lacassin, T. T. Phan, M. Brunel, and D. Seward (2000), Long and complex thermal history of the Song Chay metamorphic dome (northern Vietnam) by multi-system geochronology, *Tectonophysics*, *321*, 449–466.

Roger, F., N. Arnaud, S. Gilder, P. Tapponnier, M. Jolivet, M. Brunel, J. Malavieille, Z. Xu, and J. Yang (2003), Geochronological and geochemical constraints on Mesozoic suturing in east central Tibet, *Tectonics*, *22*(4), 1037, doi:10.1029/2002TC001466.

Roger, F., J. Malavieille, P. H. Leloup, S. Calassou, and Z. Xu (2004), Timing of granite emplacement and cooling in the Songpan–Garzê Fold Belt (eastern Tibetan Plateau) with tectonic implications, *J. Asian Earth Sci.*, *22*, 465–481.

Ruhl, K. W., and K. V. Hodges (2005), The use of detrital mineral cooling ages to evaluate steady state assumptions in active orogens: An example from the central Nepalese Himalaya, *Tectonics*, *24*, TC4015, doi:10.1029/2004TC001712.

Sambridge, M. S., and W. Compston (1994), Mixture modelling of multi-component data sets with application to ion-probe zircon ages, *Earth Planet. Sci. Lett.*, *128*, 373–390.

Schärer, U., P. Tapponnier, R. Lacassin, P. H. Leloup, D. Zhong, and S. Ji (1990), Intraplate tectonics in Asia: A precise age for large-scale Miocene movement along the Ailao Shan-Red River shear zone, China, *Earth Planet. Sci. Lett.*, *97*, 65–77.

Schärer, U., L. S. Zhang, and P. Tapponnier (1994), Duration of strike-slip movements in large shear zones: The Red River Belt, *Earth Planet. Sci. Lett.*, *126*, 379–397.

Searle, M. P. (2006), Role of the Red River Shear zone, Yunnan and Vietnam, in the continental extrusion of Southeast Asia, *J. Geol. Soc. London*, in press.

Shen, Z.-K., C. Zhao, A. Yin, Y. Li, D. D. Jackson, P. Fang, and D. Dong (2000), Contemporary crustal deformation in east Asia constrained by Global Positioning System measurements, *J. Geophys. Res.*, *105*, 5721–5734.

Tagami, T., R. F. Galbraith, G. M. Yamada, and G. M. Laslett (1998), Revised annealing kinetics of fission tracks in zircon and geological implications, in *Advances in Fission-Track*

Geochronology, edited by P. Van den Haute and F. De Corte, pp. 99–112, Springer, New York.

Thiede, R. C., B. Bookhagen, J. R. Arrowsmith, E. R. Sobela, and M. R. Strecker (2004), Climatic control on rapid exhumation along the Southern Himalayan Front, *Earth Planet. Sci. Lett.*, *222*, 791–806.

Upton, D. R. (1999), A regional fission track study of Thailand: Implications for thermal history and denudation, Ph.D. thesis, 312 pp., Univ. of London, London.

Wang, P. L., C. H. Lo, T. Y. Lee, S. L. Chung, C. Y. Lan, and T. Y. Nguyen (1998), Thermochronological evidence for the movement of the Ailao Shan-Red River shear zone: A perspective from Vietnam, *Geology*, *26*, 887–890.

Wang, P. L., C. H. Lo, S. L. Chung, T. Y. Lee, C. Y. Lan, and V. T. Trang (2000), Onset timing of left-lateral movement along the Ailao Shan-Red River shear zone: $^{40}Ar/^{39}Ar$ dating constraint from the Nam Dinh area, northeastern Vietnam, *J. Asian Earth Sci.*, *18*, 281–292.

Weislogel, A. L., S. A. Graham, E. Z. Chang, J. L. Wooden, G. E. Gehrels, and H. Yang (2006), Detrital zircon provenance of the Late Triassic Songpan-Ganzi complex: Sedimentary record of collision of the North and South China blocks, *Geology*, *34*, 97–100.

Whipple, K. X., E. Kirby, and S. H. Brocklehurst (1999), Geomorphic limits to climate-induced increase in topographic relief, *Nature*, *401*, 39–44.

White, N. M., M. Pringle, E. Garzanti, M. Bickle, Y. Najman, H. Chapman, and P. Friend (2002), Constraints on the exhumation and erosion of the High Himalayan Slab, NW India, from foreland basin deposits, *Earth Planet. Sci. Lett.*, *195*, 29–44.

Wobus, C. W., K. V. Hodges, and K. X. Whipple (2003), Has focused denudation sustained active thrusting at the Himalayan topographic front?, *Geology*, *31*, 861–864.

Yang, J. H., S. L. Chung, S. A. Wilde, F. Y. Wu, M. F. Chu, C. H. Lo, and H. R. Fan (2005), Petrogenesis of post-orogenic syenites in the Sulu orogenic belt, east China: Geochronological, geochemical and Nd-Sr isotopic evidence, *Chem. Geol.*, *214*, 99–125.

Yang, T. F., J. R. Wang, C. H. Lo, S. L. Chung, R. L. Tien, R. Xu, and W. Deng (1999), The thermal history of the Lhasa Block, south Tibetan Plateau based on FTD and Ar-Ar dating, *Radiat. Meas.*, *31*, 627–632.

Yin, J., J. Xu, C. Liu, and H. Li (1988), The Tibetan plateau: Regional stratigraphic context and previous work, *Philos. Trans. R. Soc. London, Ser. A*, *327*, 5–52.

Zhang, L. S., and U. Schärer (1999), Age and origin of magmatism along the Cenozoic Red River shear belt, China, *Contrib. Mineral. Petrol.*, *134*, 67–85.

Zheng, J., W. L. Griffin, S. L. O'Reilly, M. Zhang, N. Pearson, and Y. Pan (2006), Widespread Archean basement beneath the Yangtze craton, *Geology*, *34*, 417–420.